

E214 The ATLAS Experiment

Alperen Esen Benjamin Brandt
s39aesen@uni-bonn.de s08bbran@uni-bonn.de

Date of experiment: 08-09.05.2025 Handed in: 30.05.2025

University Bonn – Physics Faculty

Contents

1. Introduction	4
2. Preparation	4
3. Overview and Event Display	4
3.1. Electrons	4
3.2. Muons	6
3.3. Photons	6
3.4. τ -leptons	6
3.5. Dijets	7
4. Preparatory Questions	7
4.1. Question A: Decay of a Z^0 boson	7
4.2. Question B: Scattering reaction $e^+e^- \rightarrow \tau^+\tau^-$	8
4.3. Question C: Tree variable ptw	9
4.4. Question D: Gaussian error propagation for correlated parameters	9
5. Assignments on Particle Reactions	10
6. Measured Momentums and Energy Loss	10
7. Mystery Data Set	12
7.0.1. Event 6:	12
7.0.2. Event 11:	13
7.0.3. Event 20:	15
7.0.4. Event 45:	16
8. Calibration of Electrons	17
9. Calibration of Electron Energy	18
10. W-mass	24
10.1. Electron Calibration Verification	24
10.2. QCD scale factor and Kinematic Variables	24
10.2.1. Kinematic Variables	27
10.2.2. Final QCD scale factor	29
10.3. Cut selection	29
11. W boson mass	33
11.1. Gauge curves	33
11.2. Adjusting cuts and fit range	35
12. Systematic uncertainties	36
12.1. Calibration uncertainty	36

12.2. QCD scale factor uncertainty	37
12.3. Fit range uncertainty	37
12.4. Cut Selection	37
12.5. Total systematic uncertainty	37
13. Discussion	38
13.1. Part 1	38
13.2. Part 2	38
A. Appendix	39
B. A. Muon Energies in the Detectors	39
C. B. Muon Energies in the Detectors	42
C.0.1. Full η cuts in <code>ElecCalib.c</code>	42
C.0.2. Energy and η cuts in <code>ElecCalib.c</code>	42
C.0.3. Coarse η cuts in <code>ElecCalib.c</code>	43
D. W-mass	44
References	46

1. Introduction

The aim of this experiment is to analyze particle physics processes over real and simulated events from the ATLAS experiment. The study began by learning how particles leave their tracks in the detector, sample data for electron, muon, photon, tau and jet events were examined. Then, the energy losses of muons were analyzed, and electron-positron pairs from Z boson decays were used for calibration purposes. Finally, event-based interpretations were made on the data set called the “mystery dataset” and possible Standard Model processes were tried to be determined. Then Z boson mass calbraiton tried to achieved to use for measuring the W boson mass.

2. Preparation

3. Overview and Event Display

Before starting to main task of this experiment, initially event display of the particle reactions were investigated. For this purpose, five different data sets searched and tried to be familiarised to how particles reaction visualized on the display. These learning data sets are not real data sets and can be listed as electrons, muons, photons, τ leptons and jets [7].

Event display mainly shows the crosssection of the detectors and tracking systems as can be seen from fig.1. From center of the detector to outside, components of the ATLAS detector consists of Pixel Detector, Semi-Conductor Tracker (SCT), Transition Radiation Detector (TRT) in the inner part which is inside area of the green circle on event display. Following these components, there are electromagnetic calorimeter (ECAL) and hadronic calorimeter (HCAL) which are shown green and red areas on the event display consecutively. Finally, the outermost layer is the muon detector system, or muon spectrometer [7].

3.1. Electrons

On the fig.1a, the reaction of an electron with the ECAL of the ATLAS detector can be seen. When a single electron is produced in the ATLAS detector, it first leaves a clear track in the inner detector (light blue line). This track is formed due to the charge of the electron, and the direction and magnitude of its momentum are measured from this track. Then, when the electron hits the ECAL, it produces an intense electromagnetic shower (yellow area in ECAL). This shower is measured by using liquid Argon (LAr) and the energy of the electron is determined. Typically, electrons leave very little energy in the HCAL, therefore, this is a criterion for distinguishing between electrons and hadrons.

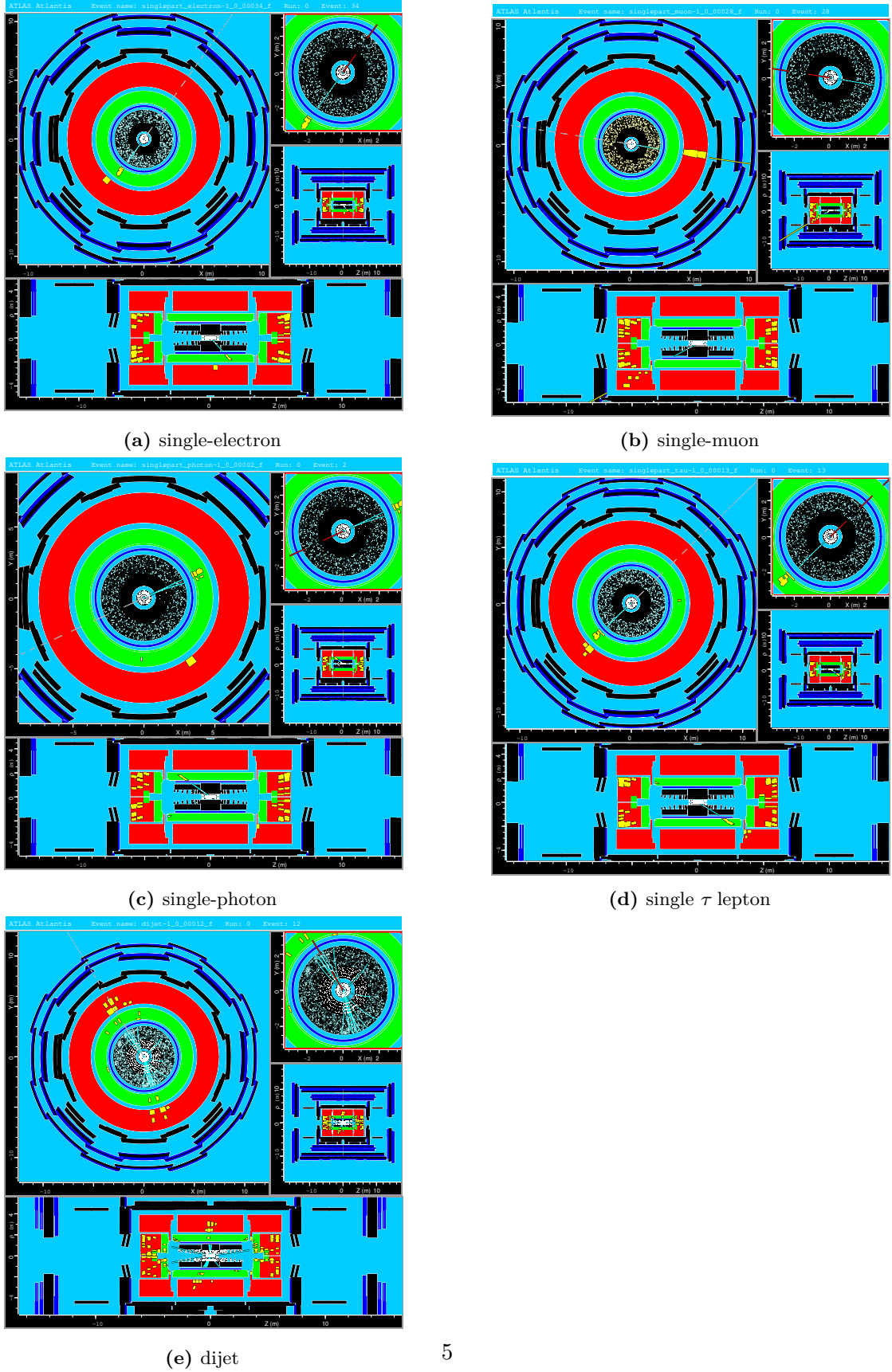


Figure 1: Event display images of ATLANTIS program for five different learning data sets.

3.2. Muons

When a muon is produced in the ATLAS detector, it first leaves a regular track as a charge-carrying particle in the inner detector system (light blue line) as seen in the fig.1b. However, unlike electrons, muons leave very little energy in ECAL and HCAL, because they interact weakly in these environments and pass through without losing most of their energy. Therefore, minimal energy accumulation is seen in the calorimeters in a muon event. After the muons pass through these layers, they are detected by the muon spectrometer, which is located in the outermost part of the detector and is specifically designed to detect muons. Here, their tracks (yellow line on fig.1b) are measured again under large magnetic fields and their charges and momentums are determined. In this way, the match of the tracks seen in both the inner detector and the muon system confirms the presence of a muon.

3.3. Photons

When a photon enters the ATLAS detector, it does not leave a trace in the inner detector system because it does not carry an electric charge. However, when it reaches the ECAL, it creates electron-positron pairs there, initiating an electromagnetic shower (EM shower). This shower expands within the ECAL, producing secondary particles, and the detector measures the energy left by these particles. If the photon has a high energy, the shower can be noticeable. The photon has little effect on the hadronic calorimeter (HCAL), because it does not interact with the hadrons. If a photon is to be confused with another particle that behaves like an electron, a trace is investigated in the inner detector. Therefore, if an EM shower is observed but no trace is found in the inner detector, this is a photon signature. On the other hand, sometimes photons interact with the inner detector and creates electron-positron pairs, and these particles also creates an EM shower on the ECAL [2]. This seems the case in the fig.1c. Because there are traces in the inner detectors.

3.4. τ -leptons

τ -leptons are the heaviest leptons in the Standard Model and have very short lifetimes (about 10^{-13} seconds). Therefore, they are not directly observed in the ATLAS detector because they decay before reaching the active regions of the detector. τ -leptons decay to produce either an electron or a muon and a neutrino which is called as leptonic decay, or several hadrons and a neutrino called as hadronic decay. In leptonic decays, the resulting electron or muon is directly observed in the detector, and the neutrino is not visible in the detector, contributing to missing transverse energy, \cancel{E}_T . In hadronic decays, a narrow hadronic jet is observed. This jet is usually narrower than ordinary QCD jets and can be distinguished by this feature. Therefore, τ -leptons are indirectly detected in ATLAS by combinations of decay products and \cancel{E}_T . In the fig.1d, a neutrino trace (dashed line) is observed, and in the reverse direction there are energy accumulation on ECAL and HCAL. It is hard to understand without knowing energy accumulation in ECAL and HCAL, if this is a hadronic or leptonic decay of τ .

3.5. Dijets

Dijet events consist of two hadronic structures (jets) that are produced by the scattering of two quarks or gluons in proton-proton collisions, and forming a jet. In the ATLAS detector, these jets are observed as large energy deposits in the HCAL, because the quarks and gluons produce large numbers of particles as they transform into hadrons, or called as hadronization. The jets may also left some energy in the ECAL, but most of the energy is absorbed in the HCAL. \cancel{E}_T in such events is usually low because all the energy can be measured by the detector. Dijets usually shows themselves as pairs of symmetric high-energy jets as can be seen from the fig.1e.

4. Preparatory Questions

In the following questions were asked for a preparation to main part of the lab, and answered as follows.

4.1. Question A: Decay of a Z^0 boson

Which value does the momentum of an electron have in the decay of a Z^0 boson $Z^0 \rightarrow e^+e^-$, if the Z^0 is at rest? [7]

In the process of decaying of Z^0 , a pair of an e^- and a e^+ is obtained, and during this process 4-vector momentum must be conserved as in eqn. 1.

$$\mathbf{P}_{Z^0} = \mathbf{P}_{e^+} + \mathbf{P}_{e^-} \quad (1)$$

more explicit way eqn. 1 can be written as,

$$\begin{pmatrix} M_{Z^0} \\ 0 \\ 0 \\ 0 \end{pmatrix} = \begin{pmatrix} E_{e^+} \\ p_{e_x^+} \\ p_{e_y^+} \\ p_{e_z^+} \end{pmatrix} + \begin{pmatrix} E_{e^-} \\ p_{e_x^-} \\ p_{e_y^-} \\ p_{e_z^-} \end{pmatrix} \quad (2)$$

Initially, Z^0 boson is at rest, hence, $E_{Z^0} = M_{Z^0}$. On the other hand, obtained e^- and e^+ have same amount of momentum but in opposite directions due to the momentum conservation ($\mathbf{p}_{e^+} = -\mathbf{p}_{e^-}$), and have same amount of energy, ($E_{e^+} = E_{e^-} = E_e$). Therefore, relation in the below eqn. 3 can be obtained from eqn. 2.

$$E_e = \frac{M_{Z^0}}{2} \quad (3)$$

using energy momentum relation, $E^2 = p^2 + M^2$, the electron momentum after decaying process can be obtained as,

$$p_e = \sqrt{E_e^2 + M_e^2} \quad (4)$$

implementing eqn. 3 to eqn. 4, final result is gained as

$$p_e = \sqrt{\left(\frac{M_{Z^0}}{2}\right)^2 + M_e^2} \quad (5)$$

Mass of the Z^0 boson has a value of $M_{Z^0} = 91.1876 \pm 0.0021 \text{GeV}/c^2$ [6], and mass of the electron has a value of $M_e = 0.51099895069(16) \text{MeV}/c^2$ [3].

Hence, $p_e = 45.5966 \pm 0.0011 \text{Gev}/c$. In this calculation, M_e negligibly small when compared to M_{Z^0} so the electron and positron almost has a momentum of the half of the Z^0 boson mass in decaying process.

4.2. Question B: Scattering reaction $e^+e^- \rightarrow \tau^+\tau^-$

How large is the momentum of tau leptons in the reaction $e^+e^- \rightarrow \tau^+\tau^-$, if the reaction takes place in the center-of-mass system (center-of-mass energy = 5 GeV)? [7]

In the scattering process of $e^+e^- \rightarrow \tau^+\tau^-$ in the fig.2, 4-vector momentum again must be conserved.

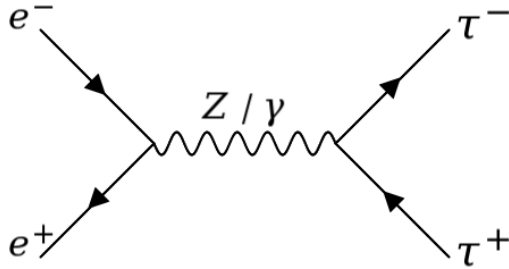


Figure 2: Feynman diagram of $e^+e^- \rightarrow \tau^+\tau^-$

$$\mathbf{P}_{\text{CM}} = \mathbf{P}_+ + \mathbf{P}_- \quad (6)$$

\mathbf{P}_{CM} is the 4-vector center of mass momentum, and can be defined as in eqn. 7,

$$\mathbf{P}_{\text{CM}} = \begin{pmatrix} E_{CM} \\ 0 \\ 0 \\ 0 \end{pmatrix} \quad \mathbf{P}_+ = \begin{pmatrix} E_\tau \\ p_{\tau_x^+} \\ p_{\tau_y^+} \\ p_{\tau_z^+} \end{pmatrix} \quad \mathbf{P}_- = \begin{pmatrix} E_\tau \\ p_{\tau_x^-} \\ p_{\tau_y^-} \\ p_{\tau_z^-} \end{pmatrix} \quad (7)$$

Therefore, using momentum conservation, $(\mathbf{P}_{\text{CM}})^2 = (\mathbf{P}_+ + \mathbf{P}_-)^2$, eqn. 10 is obtained.

$$E_{CM}^2 = (2E_\tau)^2 \quad (8)$$

$$E_{CM}^2 = 4m_\tau^2 + 4p_\tau^2 \quad (9)$$

$$p_\tau = \frac{1}{2} \sqrt{E_{CM}^2 - 4m_\tau^2} \quad (10)$$

$m_\tau = 1777.09 \pm 0.14 \text{ MeV}/c^2$ [1], and $E_{CM} = 5 \text{ GeV}/c^2$ [7]. Hence, momentum of the τ -leptons are

$$p_\tau = 1.75839 \pm 0.00056 \text{ GeV}/c^2 \quad (11)$$

4.3. Question C: Tree variable ptw

As before, the analysis is based on ROOT trees. One of the tree variables is ptw - the estimated transverse momentum of the W boson candidate. This variable can be constructed from the other tree variables. Please think about how this could be done. [7]

The transverse momentum of the W boson, is can be described with the electron momentum and the neutrino momentum

$$\vec{p}_{T,W} = \vec{p}_{T,e} + \vec{p}_{T,\nu}$$

The transverse momentum of electron and neutrino is made up of a part in x and a part in y direction. So the value of the $|\vec{p}_{T,W}|$ can be calculated using

$$|\vec{p}_{T,W}| = \sqrt{(p_{T,e,x} + p_{T,\nu,x})^2 + (p_{T,e,y} + p_{T,\nu,y})^2}.$$

Since the neutrino momentum can't be measured directly in the detector, this missing transverse momentum is used. Inserting the corresponding ROOT variables in the expression, $|\vec{p}_{T,W}|$ can be constructed with

$$\text{ptw} = \sqrt{(\text{el_px} + \text{ptmissx})^2 + (\text{el_py} + \text{ptmissy})^2}.$$

4.4. Question D: Gaussian error propagation for correlated parameters

Please look up the correct form of the Gauss error propagation law in the presence of correlations. You will need that for the final error on the W mass. [7]

If a function $f(a,b)$ has uncertainties σ_a and σ_b , which are correlated, the gaussian error propagation for correlated uncertainties is given by

$$\sigma_f^2 = \left(\frac{\partial f}{\partial a} \cdot \sigma_a \right)^2 + \left(\frac{\partial f}{\partial b} \cdot \sigma_b \right)^2 + 2 \cdot \frac{\partial f}{\partial a} \cdot \frac{\partial f}{\partial b} \cdot \sigma_{ab}$$

5. Assignments on Particle Reactions

6. Measured Momentums and Energy Loss

In order to investigate the energy loss of muons, energy measurements of 20 consecutive events in the `muon learning` dataset were compared. In this analysis, the differences between the momentum measured in the inner detector and the momentum measured in the muon spectrometer were evaluated. Both detectors determine the momentum by following the trajectory of the muons with the help pf a magnetic field. Transverse, p_T , and total momentum, p , values are derived from the curvature of the curved track of the charged particle. These values were obtained from the each event using `ATLANTIS` program.

The dataset was selected to include as many consecutive events as possible. However, since the detectors could not detect the energy measurement in some events, these events were excluded from the analysis. In particular, missing measurements were detected in events 3, 10, 14 and 21, and this data set can be seen in the tab.9 and tab.10. The measured negative momenta are generally associated with μ^- , and the positive momenta with μ^+ . Thus, the momenta observed in each event also contributes to the indirect determination of the particle's charge.

In the fig.3, the events belonging to muons are analyzed. The horizontal axis shows the event number, while the vertical axis shows the difference between the momentum measured in the inner detector and the momentum measured in the outer muon detector for each event, or the energy loss. This difference is usually positive due to the weak interaction of muons with the detector materials, since muons mostly lose their energy through ionization. The red horizontal line in the graph represents the average energy loss and equal to $3 \pm 6\text{GeV}/c^2$. The light magenta band shows the standard deviation range of $\pm 1\sigma$, and determined by the Gaussian error propagation. Remarkably, all measurements except 3 data points intercept with this band. This shows that the measurements largely follow the expected statistical distribution.

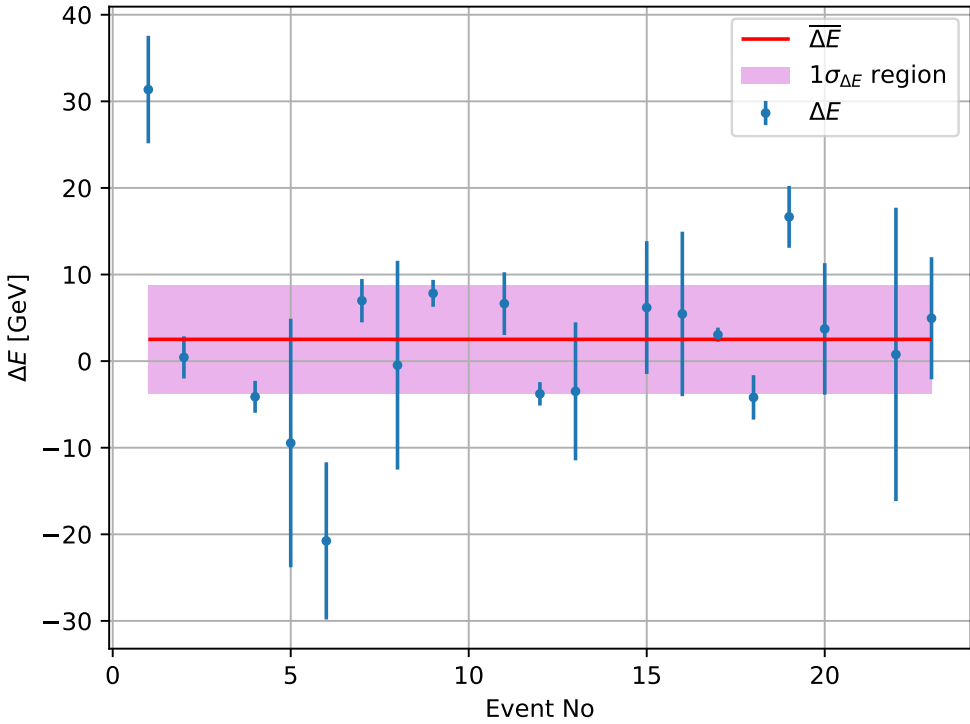


Figure 3: Energy loss of muons in the ATLAS detector corresponding to each event number. Red lines shows the average energy loss, and most of the measurements stand inside the $\pm 1\sigma$ error range.

However, in some events the energy difference is negative. This situation can occur for various reasons. First, it can be due to systematic errors in the momentum measurement or differences in detector resolution. In particular, although the magnetic field in the inner detector provides a more sensitive measurement, deviations can occur. A second possibility is that the momentum measurement in the outer detector appears higher than it actually is due to magnetic field or timing differences. Finally, particle tracks or residual signals within the event may also disturb the measurement in the outer detector.

Even though errors for p_T were provided by the ATLANTIS program, errors for total momenta, p was not provided. It is assumed that error propagation of the transverse momentum, p_T , is the same with error propagation of total momentum. Therefore, errors for total momentum calculated as in eqn.12.

$$\frac{\sigma_{p_T}}{p_T} = \frac{\sigma_p}{p} \quad (12)$$

7. Mystery Data Set

The dataset named `Mystery-xxx.dat` was prepared to examine possible physical processes in the Standard Model. A pre-selection was applied to this dataset in advance, and it is known that at least two leptons (e and μ) are present in each event. The aim of this study is to determine which Standard Model process could cause these events by using the distinctive features of the leptons, jets, or E_T [7]. For this purpose, events numbered 6, 11, 20, and 45 were selected and examined.

7.0.1. Event 6:

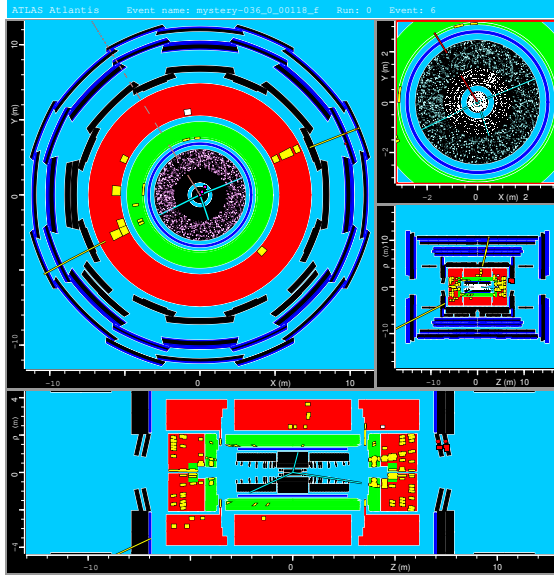


Figure 4: Mystery data set Event 6

Two muons are observed in this event. Since the E_T was measured as 2.082 GeV which is quite small, the probability of a neutrino presence in the event is low. Also, the muons are moving in opposite directions. This suggests that the event may be a Drell-Yan process for pair production as can be seen from fig.5. In this process, a virtual photon, γ^* or Z boson is created by the scattering of one quark anti-quark pair, then this boson (or photon) decays into a lepton pair (here two muons). If the event was a W boson, a neutrino would be expected among the decay products. However, the low E_T observed indicates that there is no such neutrino contribution.

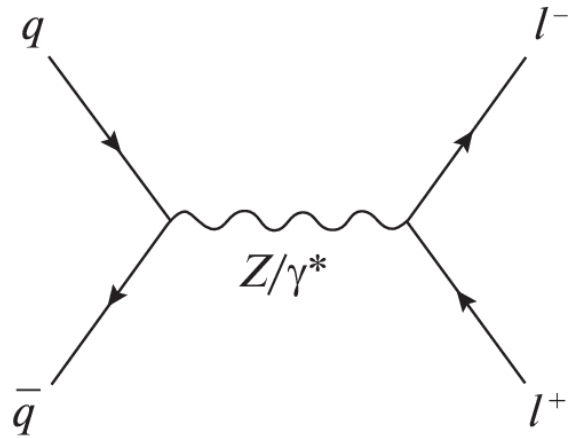


Figure 5: Drell-Yan Processes of a Z -boson or photon decaying to a lepton pair. Figure was taken from [5]

Also, it must be noted that these two particles deposited low energies on the calorimeters. For left muon deposited energy smaller than 5 GeV, and for right muon smaller than 3 GeV. On the other hand, p_T was measured for right muon as -21.83 ± 1.413 GeV, and for left muon as 45.06 ± 3.807 GeV. These opposite signed energy values shows that these two particles have opposite charges, and smaller deposited energies on the calorimeters also shows that these two particles are actually muons.

7.0.2. Event 11:

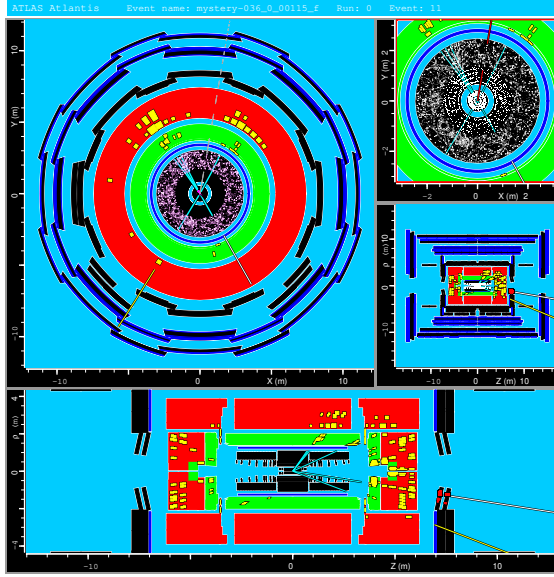


Figure 6: Mystery data set Event 11

On the upper side of the event display, there are two jets formations are seen. On the bottom side again two muons were observed due to same reasons before: small energy deposition on calorimeters and high p_T values can be seen from below tab.2

product	Energy information [GeV]
bottom left μ	$p_T = -41.55 \pm 5.129$
bottom right μ	$p_T = 121.40 \pm 3.258$
top left jet	21.1(ECAL) 37.0(HCAL)
top right jet	8.9(ECAL) 19.5(HCAL)
possible ν	$\not{E}_T = 23.773$

Table 1: Energy information of particles in Event 11, values were obtained via ATLANTIS program

This process cannot be basically leptonic pair production from Z boson or a photon. Because there are two jet formations and a possible neutrino were observed besides two muons. Possible processes can be considered as quark and antiquark scattering or gluon-gluon fusion can be described as in the eqn.13, and eqn.14. Feynman diagrams of these processes can be seen from the fig.7.

$$q\bar{q} \rightarrow g \rightarrow t\bar{t} \rightarrow bW\bar{b}W \rightarrow b\mu\nu_\mu\mu\nu_\mu\bar{b} \quad (13)$$

$$gg \rightarrow b\bar{b}b\bar{b} \rightarrow bZWC \rightarrow b\mu^+\mu^-e\nu_e c \quad (14)$$

In the eqn.13, two b quarks can be the responsible from the jet formations and there is chance that one of the neutrino could not be detected.

Same in eqn.14, one b and one c quarks can be responsible from the jet formations, and the e could not be detected.

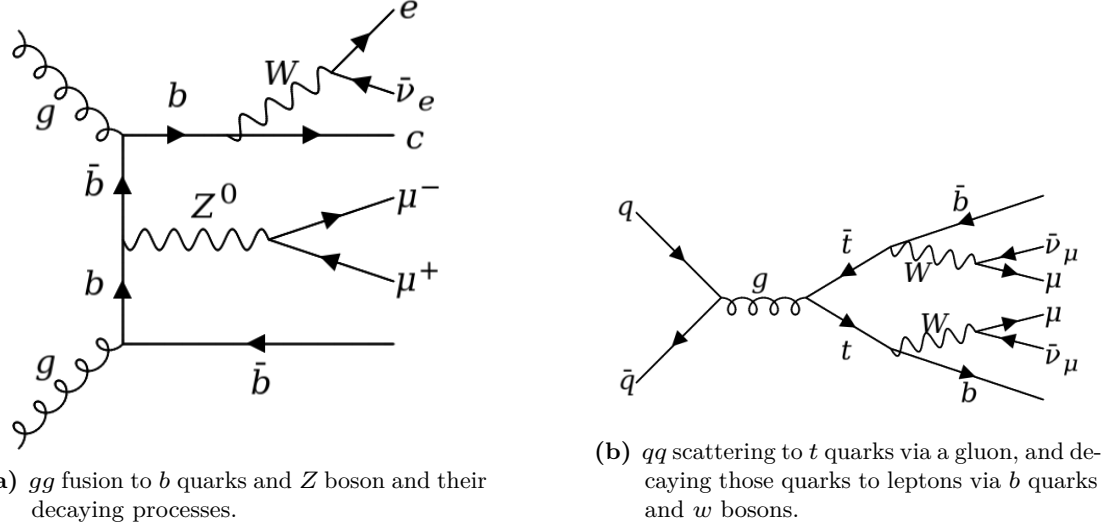


Figure 7: Possible hard scattering processes for Event 11

7.0.3. Event 20:

In this event 8, \cancel{E}_T has a value around 60 GeV which shows the presence of a neutrino in this event. Also, on the right top there is a muon observed because it was detected on the muon spectrometer, and it deposit less energy around 2.2GeV. On the right top part of the display, there is a particle which createad a EM shower on the ECAL, but no signnnificant energy deposited on the HCAL. This particle could be a photon, positron, or an electron. However, It is known that there is always at least two leptons in each event, it is highly possible that this particle is not a photon. Because, there is no other muon detection and any other energy deposition on the ECAL, no other lepton candidate left on the display except the one create an EM shower on the top left. To sum up, in this event one e^- (or e^+), one muon and one neutrino is obtained. This process can be explained by the weak interaction processes. For instance, b quark decay as in eqn.15.

$$b \rightarrow Wc \rightarrow e\nu_e Ws \rightarrow e\nu_e \mu\nu_\mu s \quad (15)$$

This process can be seen from the fig.9.

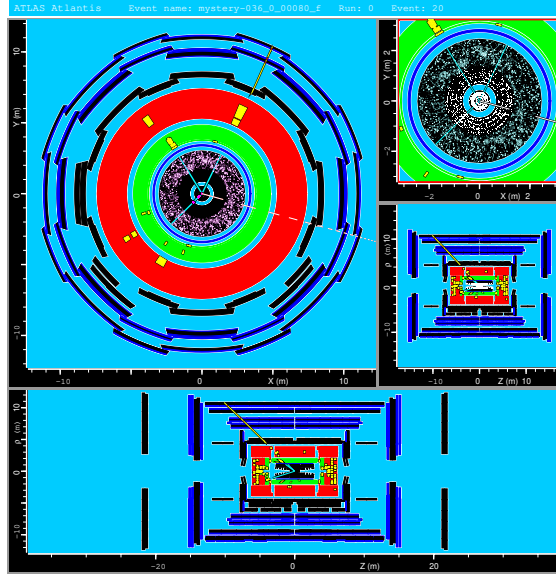


Figure 8: Mystery data set Event 20

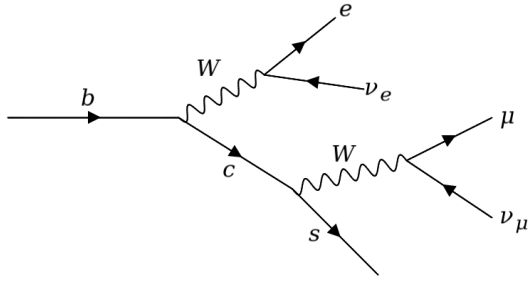


Figure 9: b quark decay to weak interaction particle of W bosons

7.0.4. Event 45:

In Event 45 in the fig.10, a high energy muon (p_T equal to 81.3 ± 7.8 GeV) and a significant \cancel{E}_T of about 49 GeV are observed, indicating the presence of a neutrino. In addition, there are two jet candidates in the event. Both of them deposited energy in both ECAL and only right bottom jet deposited energy on the HCAL, suggesting hadronic behavior. The jet bottom left appears to be an EM shower instead of a jet and it seems in the same track as the muon. These features point to a top quark decay scenario involving leptonic W boson decay together with hadronic fragmentation originating from a b -quark ($t \rightarrow bW \rightarrow b\mu\nu$). Therefore, the claim that the event originated from a top-quark pair production process ($t\bar{t} \rightarrow b\mu\nu\bar{b} + X$ as can be seen from fig.7b) is strongly supported.

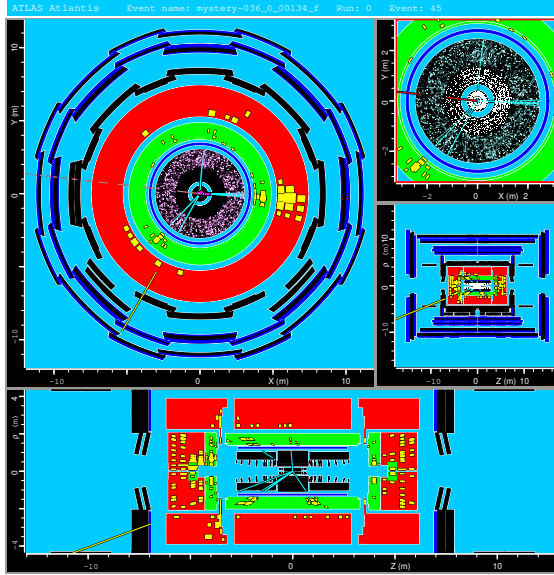


Figure 10: Mystery data set Event 45

product	Energy information [GeV]
bottom left μ	$p_T = 81.28 \pm 7.768$
bottom left jet	52.4(ECAL) 3.0(HCAL)
bottom right jet	65.3(ECAL) 24.0(HCAL)
ν	$E_T = 48.891$

Table 2: Energy information of particles in Event 11, values were obtained via ATLANTIS program

8. Calibration of Electrons

Measuring the energy of electrons in an ECAL is the most sensitive way to determine their energy. However, the raw energy measurements given by the detector do not directly give accurate results and these data must be calibrated. The main reason for this is that the calorimeter consists of many parts and the energy responses of these parts may differ slightly from each other. In addition, electrons may lose energy in other areas of the detector before reaching the calorimeter, or some energy may be absorbed in the passive regions of the calorimeter. Due to these systematic effects, the ATLAS data sets provided in the laboratory contain only raw energy measurements, and these measurements are usually lower than the actual energy of the electron. Therefore, the electron energy must be calibrated. This calibration process will be carried out using the ROOT program in this laboratory study with the decay of Z boson as $Z \rightarrow e^+e^-$ [7]. After this calibration

done results are used to measure W boson mass accurately. Because W boson also decays leptons as $W \rightarrow e\nu$, which consists of electrons (or positrons).

9. Calibration of Electron Energy

The electron energy calibration in the ATLAS calorimeter is done using the mass distribution of electron-positron pairs from the Z^0 boson. The properties of the Z^0 boson have been measured to high precision at the LEP collider, and its mass is known with a relative uncertainty of $\sim 2 \times 10^{-6}$ GeV. Therefore, the Z^0 peak of electron-positron events is a well-known signal and is used for calibrating the detector.

In an ideal detector, the invariant mass distribution $F(M_{ee})$ is modeled as:

$$F(M_{ee}) = \frac{a}{M_{ee}^2} \left(\frac{1}{(M_{ee}^2 - M_Z^2)^2 + M_Z^2 \Gamma_Z^2} + F_{\text{Int}}(M_{ee}) + Bg(M_{ee}) \right) \quad (16)$$

Here M_Z is the nominal mass of the Z^0 boson, Γ_Z is the decay width. $F_{\text{Int}}(M_{ee})$ is the γZ^0 interference term, and $Bg(M_{ee})$ is the background due to misidentified leptons[7]. Two approximation made, first one is γZ^0 term is neglected, and second, standard Breit-Wigner, eqn.17 is used instead of relativistic one which is the 1st term in the brackets in the eqn.16

$$F(M_{ee}) = \frac{\Gamma_Z^2/4}{(M_{ee} - M_Z)^2 + \Gamma_Z^2/4} \quad (17)$$

So, using the eqn.16 with eqn.17, χ^2 fit is applied and plot in fig.11 was obtained.

The effect of this approach on the measurement is negligible. However, detector effects can systematically disturb the energy distribution by broadening this narrow peak. Depending on the region where the electron enters the calorimeter, the measured energy may deviate from the true energy [7]. The measured energy data can be seen from fig.11. Therefore, the calibration process is of great importance to correct the systematic errors of the detector.

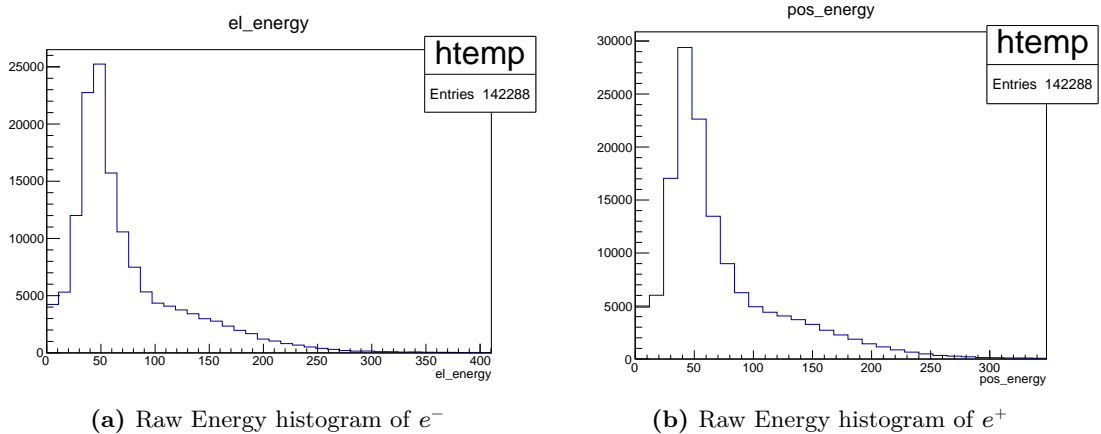


Figure 11: Raw energy distributions of elektrons and positrons. Unit of horizontal axis is GeV and vertical axis is counts. As can be clearly seen that peak points of the both graphs are located around 50GeV which is almost half of the mass of Z boson

Using the **ROOT** commands, necessary bins are applied to electron mass distribution. Positron mass distribution is similar to electron mass distribution, so separate binnings were not applied to positron mass distribution. Without any binning selection, mass distribution of Z boson can be seen from fig.12.

Here energy calibration done with a calibration factor defined as (M_Z^{real}/M_Z^{meas}) . When this calibration factor multiplied with raw energy, calibrated energy is obtained. M_Z^{real} is the literature value which is taken to be reference to Z^0 boson mass. M_Z^{meas} is measured Z^0 boson mass and it is obtained with different parameters as raw energy, transverse momentum (p_T), direction of electron ϕ and η , transversal energy in the calorimeter (**etiso**), ratio of electron-raw energy and electron momentum (**eoverp**), distance of the electron to the nearest jet in the $\eta\phi$ plane (**drjet**) [7]. To do this calibration, first, energy plot with binning according to mentioned parameters done using **ROOT** commands. After looking this plot, measured energy value, M_Z^{meas} , is obtained and calibration parameter is calculated. For instance, M_Z^{meas} value for $0.5 < |\eta| < 1.0$ is obtained from plot in the fig.13 as 89.82 ± 0.04 GeV.

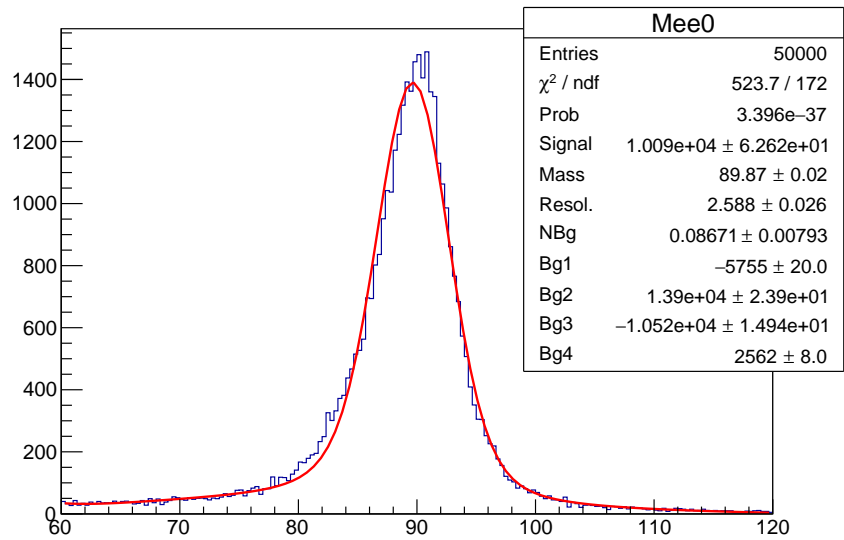


Figure 12: Raw Z mass distribution. Fit is applied according to convolution of a Gaussian function with a Breit-Wigner function which is eqn.17. Unit of horizontal axis is GeV, vertical axis is counts.

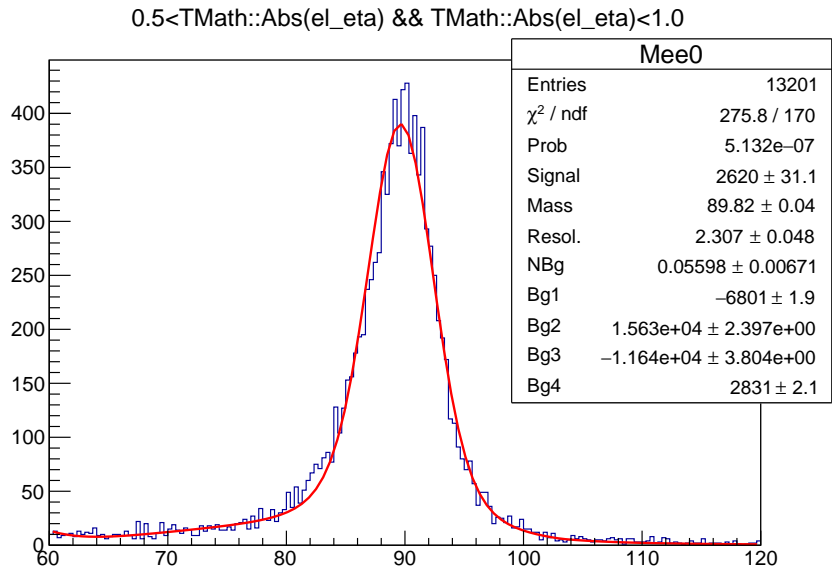


Figure 13: Z mass distribution with $0.5 < |\eta| < 1.0$. Unit of horizontal axis is GeV, vertical axis is counts.

Initially, we have 89.87 ± 0.02 GeV for Z boson mass. This value has been tried to be improved for the exact value $M_{Z^0} = 91.1876 \pm 0.0021$ GeV/ c^2 [6] with better χ^2/ndf value which has to be approximately around 1 for an ideal case. Following procedures were applied for improvement.

First, in the full η range were bin with each 0.2 increment which is considered as fine binning. Full code for this binning and the following ones can be seen in sec.C.

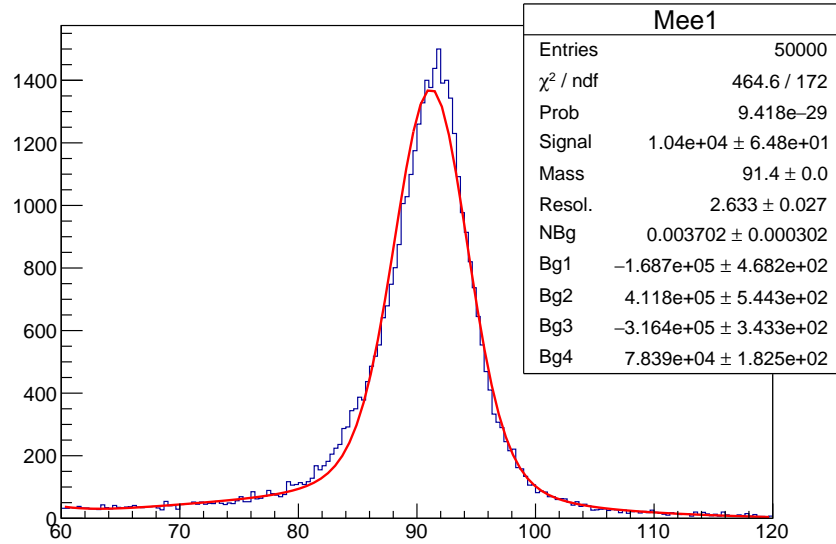


Figure 14: Z mass distribution with fine binning of η . Unit of horizontal axis is GeV, vertical axis is counts.

As seen from the fig.14, Z boson mass calculated as 91.4 ± 0.0 GeV after fine cut. It was thought that energy value may be improved binning with two different parameters, and η and raw energy values are used.

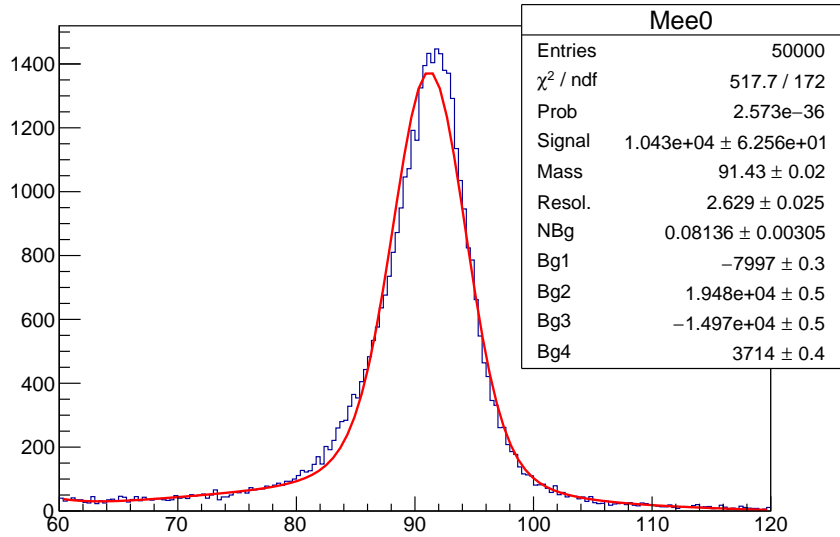


Figure 15: Z mass distribution with raw energy and η binnings. Unit of horizontal axis is GeV, vertical axis is counts.

For each 0.5 increment of η , full energy range was binned from 30 GeV to 70 GeV with increment of 10 GeV in a nested loop, and can be seen from sec.C. After this binning, plot in fig.15 was obtained. Here, in fig.15, 91.43 ± 0.02 GeV. The obtained result getting worse with this approach so decided to stick one parameter, and after couple of trying on different parameters such as azimuthal angle ϕ and transverse momentum p_T , we decided to use η .

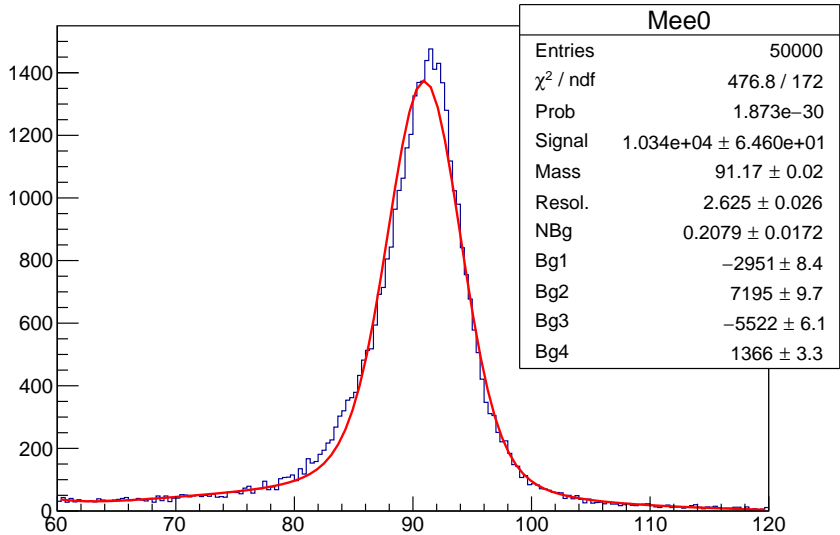


Figure 16: Z mass distribution with coarse η binnings. Unit of horizontal axis is GeV, vertical axis is counts. This distribution result used as calibration.

However, this time η binned coarsely as 0.5 increments as can be seen from the tab.3, also corresponding C code in `ElecCalib.c` can be seen from sec.C

Range	Energy[Gev]
$0.0 < \eta < 0.5$	$* = 91.2/90.18$
$0.5 < \eta < 1.0$	$* = 91.2/90.12$
$1.0 < \eta < 1.5$	$* = 91.2/89.80$
$1.5 < \eta < 2.0$	$* = 91.2/91.22$
$2.0 < \eta < 2.5$	$* = 91.2/88.72$

Table 3: In each absolute value of 0.5 η range, energy value is updated with approximate exact value of M_Z divided with each measured mass value M_Z according to corresponding binning of η .

Final calibrated mass of M_Z is obtained as 91.17 ± 0.02 with $\chi^2/\text{ndf} = 2.77$. Literature value of $M_{Z^0} = 91.1876 \pm 0.0021 \text{GeV}/c^2$ [6]. As expected, our error range is bigger than the literature value, however, M_Z value we obtained stays inside the error range of M_Z value taken from literature. After this result, calibration accepted as done, and our result transferred to W boson mass measurement part of the experiment by the tutor.

10. W-mass

With the finished calibration, the mass of the W-boson can now be measured. This is done using the Jacobi peak of the electron transverse momentum distribution. In order to determine the W-mass, we use a data set of actual ATLAS data containing $W \rightarrow e\nu$ events, as well as several simulated data sets also containing $W \rightarrow e\nu$ events. There is also a $Z^0 \rightarrow e^+e^-$ data set to check the validity of the previous calibration. Finally there are data sets for QCD- and non-QCD background events.

10.1. Electron Calibration Verification

First the previous calibration of the electron energy is verified by examining the $Z^0 \rightarrow e^+e^-$ data set. This is done for regions of the detector as well as for different kinematic regions. The different bins of the detector as well as the different kinematic regions that were chosen and the resulting Z^0 masses are listed in table 4. The fits to the m_{ee} spectrum can be seen in figure 17 and 18.

cut selection	$M_{Z^0,meas} / \text{GeV}$
$p_{T,e^\pm} > 40 \text{ GeV}$	91.71 ± 0.02
$p_{T,e^\pm} < 40 \text{ GeV}$	90.5 ± 0.0
$35 < p_{T,e^\pm} < 55 \text{ GeV}$	91.43 ± 0.02
$\eta > 2$	89.89 ± 0.05
$\eta < 0.5 \& p_{T,e^\pm} > 40$	91.69 ± 0.02
$\eta < 0.5 \& p_{T,e^\pm} < 40$	90.56 ± 0.03
$\phi < 0$	91.14 ± 0.02
$\phi > 0$	91.13 ± 0.02

Table 4: Measured Z^0 mass for different cut selections

Although there is some deviation from the literature value of the Z^0 mass, $m_{Z^0}^{lit} = (91.1880 \pm 0.0020) \text{ GeV}$ [4], overall the Z^0 masses are close to the literature value and deviate by less than 1%. For large η the deviation is a bit larger (1.), which is most likely due to the fact that the detector resolution is best for particles which travel perpendicular to the beam line. The more forward the final particles are, the worse the detection efficiency resolution get.

10.2. QCD scale factor and Kinematic Variables

In order to achieve an accurate measurement of the W-mass, the background processes at ATLAS have to be taken into consideration. At LHC, proton proton collisions cause the measured events, therefore the background coming from QCD processes is large. This causes a problem, since the final products of the $W \rightarrow e\nu$ events we use to measure the W-mass are leptons which do not interact with the strong interaction. This makes the simulation of a QCD background for the $W \rightarrow e\nu$ events difficult. In order to solve this

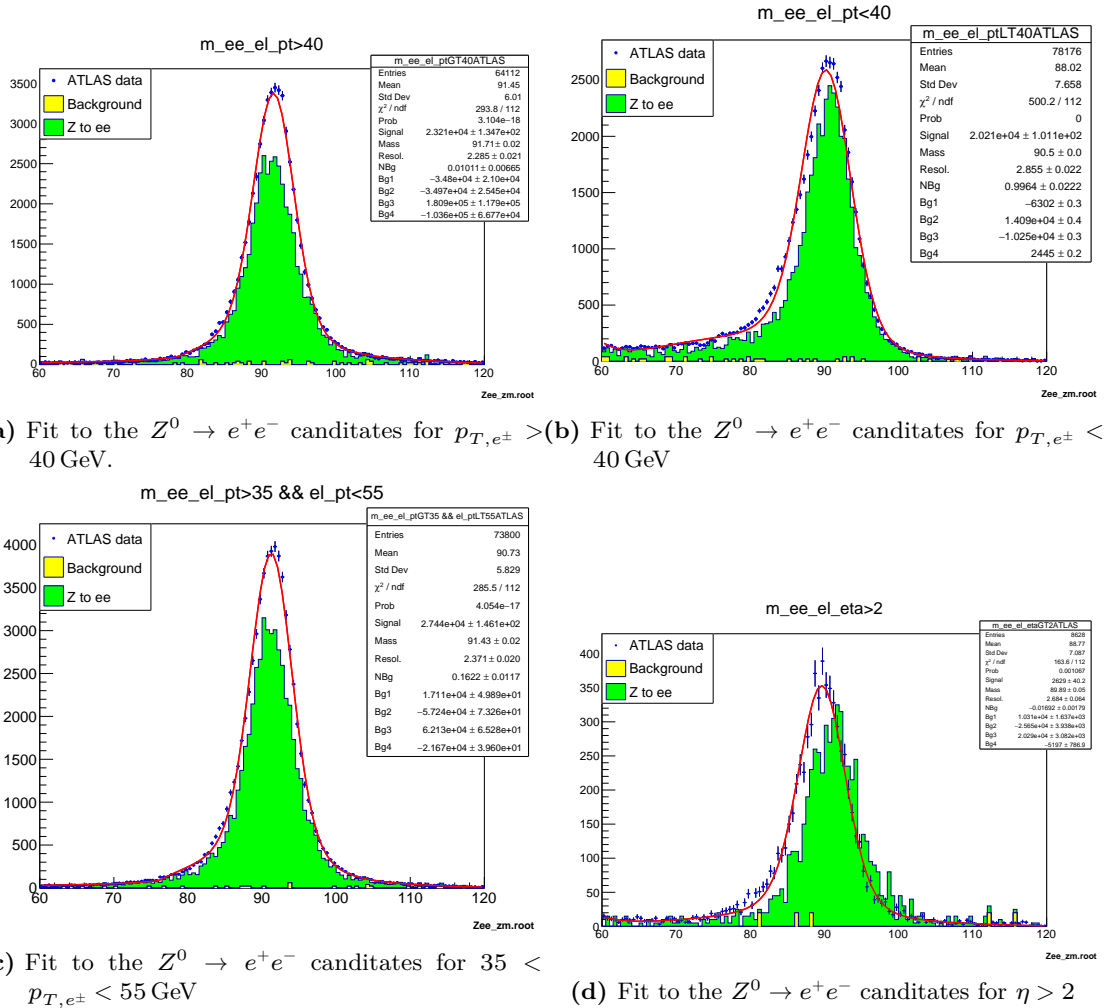


Figure 17: Fitted $Z^0 \rightarrow e^+e^-$ data for different regions of the detector as well as different kinematic regions.

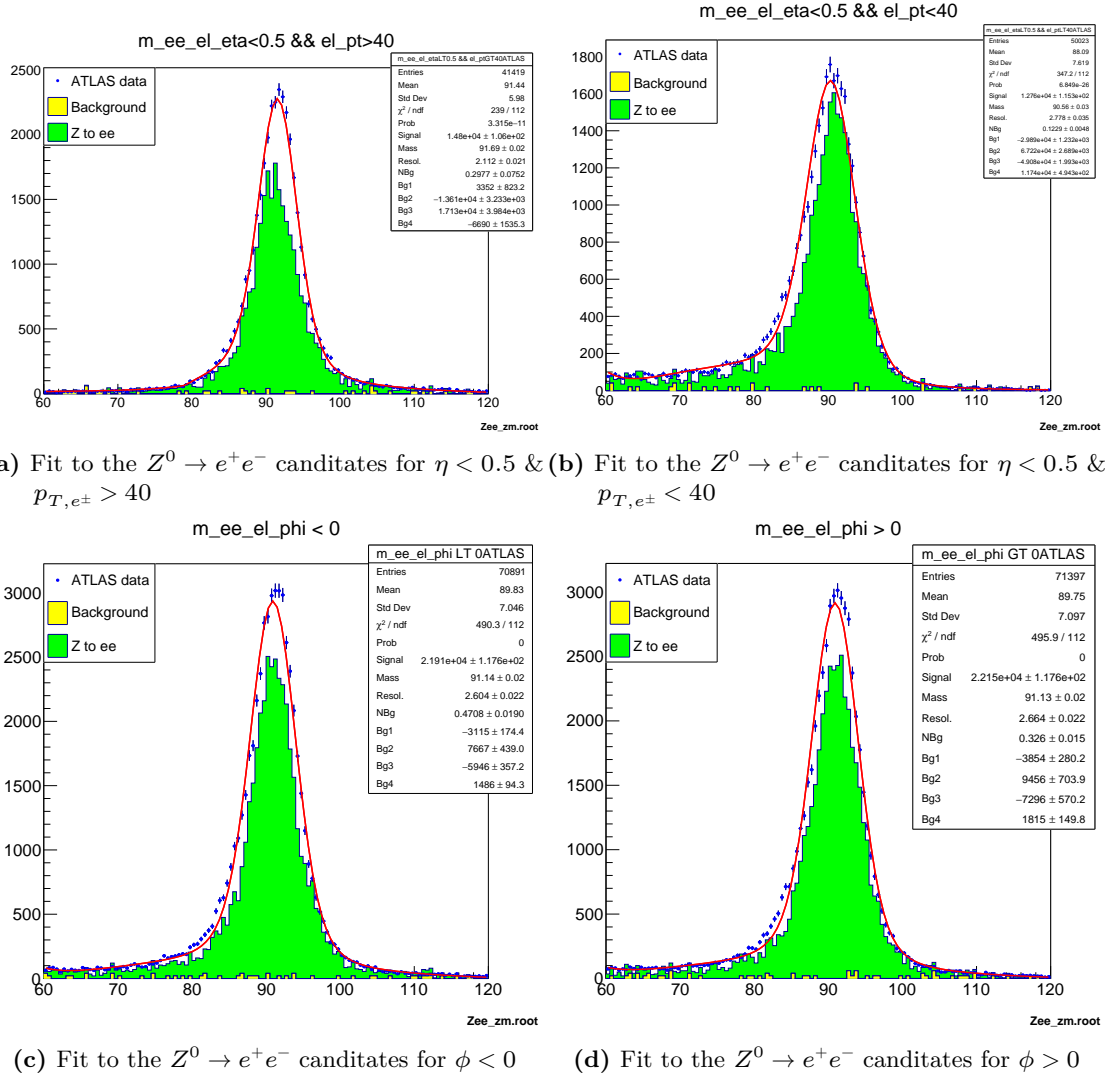


Figure 18: Fitted $Z^0 \rightarrow e^+e^-$ data for different regions of the detector as well as different kinematic regions.

problem, the QCD background is extracted from the data. In order to scale the data correctly, a QCD scale factor is used, since the integrated luminosity of the background is not measured and therefore unknown. In order to get an understanding of the QCD scale factor and its effect on the data, different kinematic values are plotted for different QCD scale factors.

10.2.1. Kinematic Variables

In order to get a feeling for the QCD scale factor and estimate its optimal value, different kinematic Variables are analyzed. The chosen kinematic variables are `el_pt` (the transverse momentum of the electron), `etmis` (missing transverse energy/momentun), `njet` (number of jets in the event) and `ptw` (transverse momentum of the W boson). The distributions of these different variables for a scale factor of 1 (meaning no scaling) can be seen in figure 24. From figure 24 it is obvious that the ATLAS data does not agree very well with the simulations. In order to solve this, the QCD scale factor was set to different values whilst looking at the distributions until the agreement between real and simulated data was optimal by eye. Compromises were necessary, since the alignment between real data and simulated data was unequal for different regions. After some trial and error, the optimal QCD scale factors the four mentioned kinematic variables were chosen as:

Variable	QCD scale factor
<code>etmis</code>	0.30 ± 0.05
<code>el_pt</code>	0.35 ± 0.07
<code>njet</code>	0.46 ± 0.08
<code>ptw</code>	0.42 ± 0.06

Table 5: Optimal QCD scale factors for each of the examined kinematic variables.

The errors were chosen to account for the previously mentioned problem, that the data aligned unequally well with the simulated data in different regions of the distributions. Therefore the errors were chosen, such that at the end of the error interval, the alignment was best in one region whilst the disalignment in the rest of the distribution was still decent. Overall the kinematic variables display the expected behavior. The transverse momentum of the W-boson `ptw` is mostly small, meaning less than ca. 30 GeV. When looking at the electron transverse momentum `el_pt`, the $W \rightarrow e\nu$ events display a peak between 40 and 50 GeV which is expected since this is around half the mass of the W-boson, which is coming from the Jacobi peak [7]. The increase towards lower p_T is mostly due to QCD background. When looking at the missing transverse momentum `etmis` the distribution behaves similarly to the electron transverse momentum `el_pt`, which is expected. Since the transverse momentum of the W-bosons is mostly small, compared to that of the from the decay resulting electron and neutrino, due to momentum conservation, the electron and the neutrino get approximately half the W-boson mass as energy. It is therefore expected that both these distributions, when disregarding the

background, feature a peak located around the W-boson mass. The distribution In the

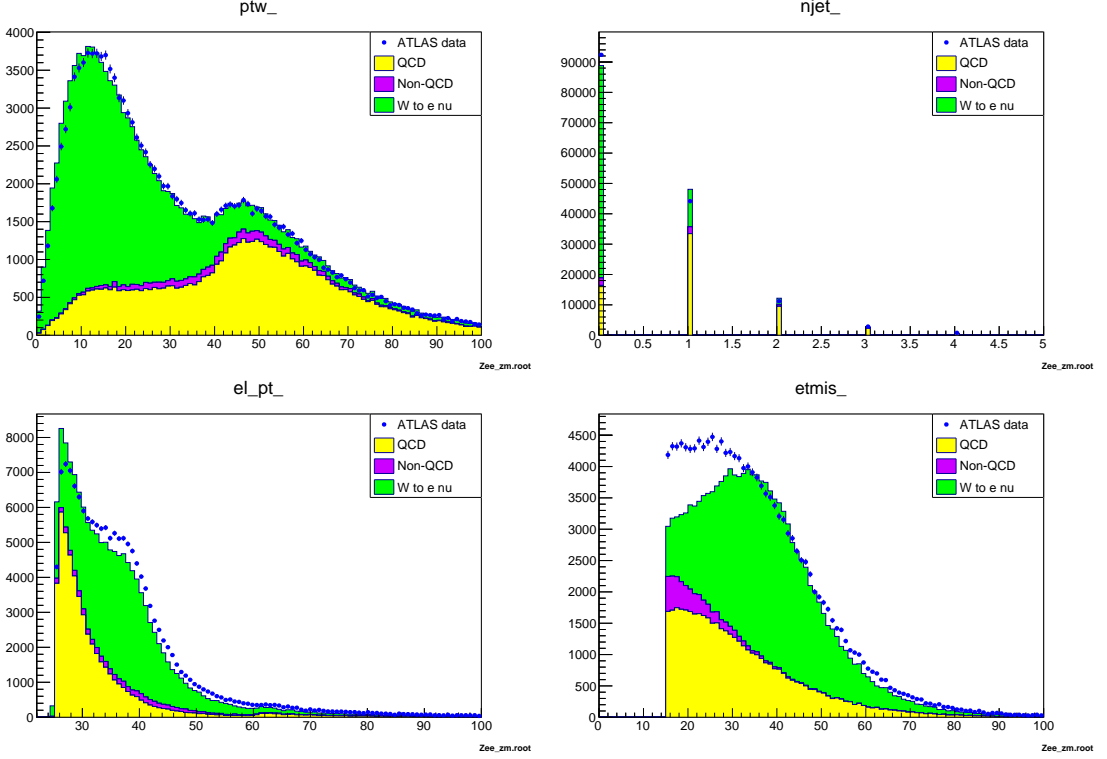


Figure 19: Distributions of the kinematic variables ptw , n_{jet} , el_pt and $etmis$ for the QCD factors mentioned in table 5

next step, the distribution of p_T^W is analyzed for events with different jet multiplicities. The corresponding histograms are displayed in figure 20. A clear trend is observed: the signal-to-background ratio decreases as the number of jets increases. This behavior aligns with the jet multiplicity distribution shown previously in figure 19.

For events with zero jets, the signal is dominant at low p_T^W , peaking around 10-15 GeV. This is expected, as there are no jets present to impart recoil to the W boson. However, when considering events with one jet, the signal drops significantly, and the previously observed peak at low p_T^W disappears. Instead, the signal appears relatively flat in the low to mid- p_T^W range and then declines at higher values. This can be explained by the presence of one jet in these signal events, which imparts recoil to the W boson. Although the jet direction is unknown, assuming an isotropic distribution, this results in a roughly uniform p_T^W distribution. Lower p_T^W values correspond to a forward jet recoil, while mid to high p_T^W suggests more transverse recoil.

The background shows a noticeable increase around 50 GeV. This could be related to the W boson mass, as the peak occurs slightly above half its mass, although other factors may also contribute.

As the number of jets increases further, the signal continues to diminish while the

background becomes more dominant. The background still peaks around 50 GeV, but the overall number of events decreases. This trend is consistent with expectations: the original process does not favor the presence of jets, and the likelihood of additional (radiated) jets decreases with increasing event complexity, due to a reduction in available vertices.

10.2.2. Final QCD scale factor

After examining the different kinematic variables, a final QCD scale factor has to be chosen. In order to do so, a region with high QCD background is chosen. For this we used the distribution of ptw , since the signal consists mostly of QCD background for energies larger than around 30 GeV, as can be seen in figure 19. Therefore the cut

$$\text{ptw} > 30 \text{ GeV}$$

is applied. To further increase the background, only events where the number of jets is larger than zero are taken into account, since we can see from figure 20, that the background to signal ratio increases for events with more than one jet. Therefore the cut

$$\text{njet} > 0$$

was also applied. When looking at the two remaining kinematic variables, el_pt and etmiss in figure 19, it can be observed, that for momenta lower than 30 GeV, the background dominates the signal. Therefore the cuts

$$\begin{aligned}\text{el_pt} &< 30 \text{ GeV} \\ \text{etmiss} &< 30 \text{ GeV}\end{aligned}$$

were also applied. The resulting distribution for different QCD scale factors can be seen in figure 21. The optimal value where the agreement between real and simulated data was identified by eye at $c_{QCD} = 0.35$. The ptw distribution for that scale factor can be seen in part (b) of figure 21. To determine the error bounds of the QCD scale factor, the QCD scale factor was varied until the simulated and real data deviated visibly. The final QCD scale factor was then chosen as

$$c_{QCD} = 0.35^{+0.04}_{-0.05}$$

Since this entire process was only done per eye, this result is highly subjective. However, in the following step, the background will be reduced as much as possible, therefore the QCD scale factor does not have a very large impact on the final result of m_W .

10.3. Cut selection

In order to achieve the most accurate m_W a cut selection has to be applied, so that the distribution of the el_pt , which is used to calculate m_W , has the highest signal to background ratio. In order to choose the proper cut selections, the distributions of the

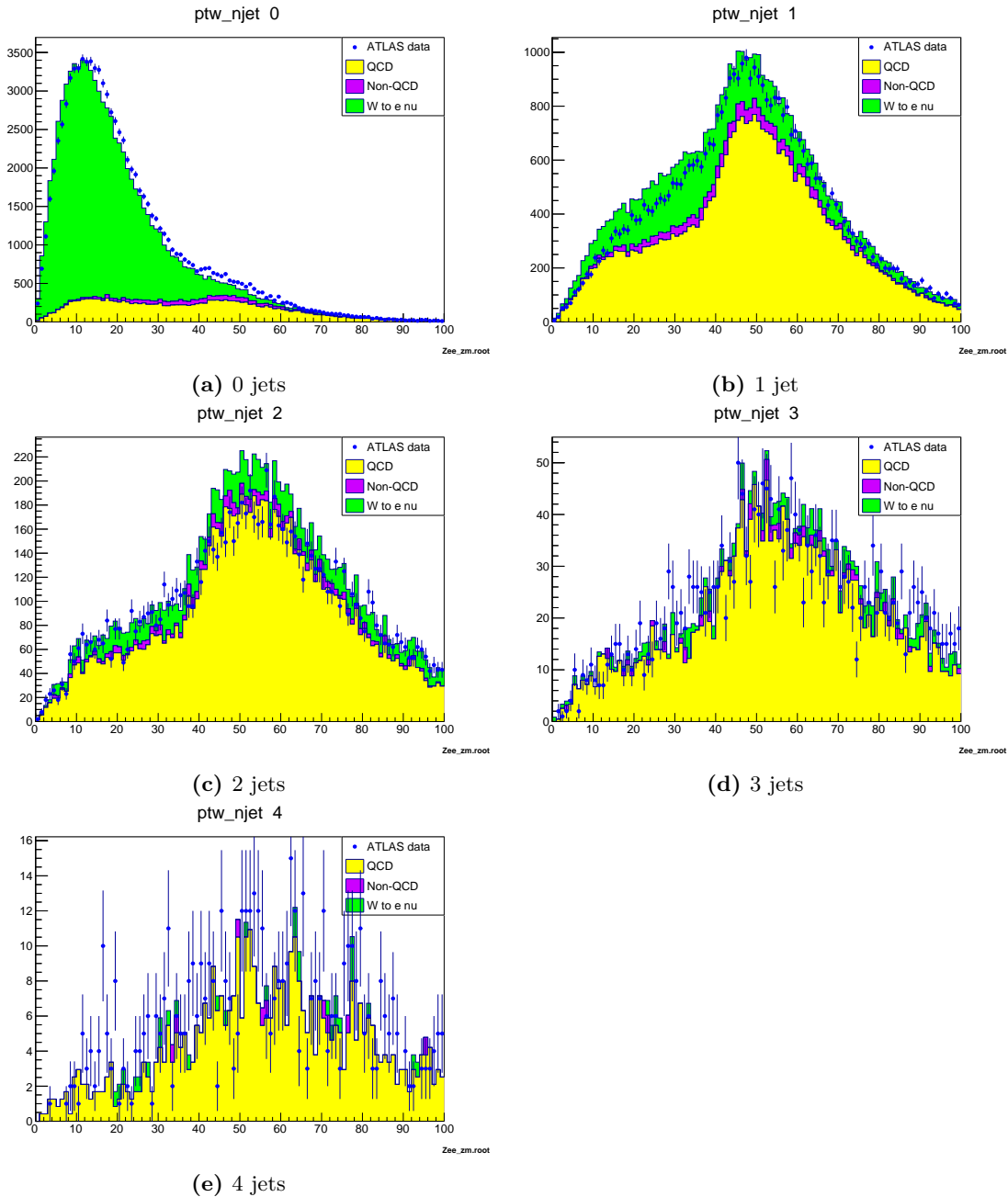


Figure 20: ptw distributions for different number of jets measured in the events

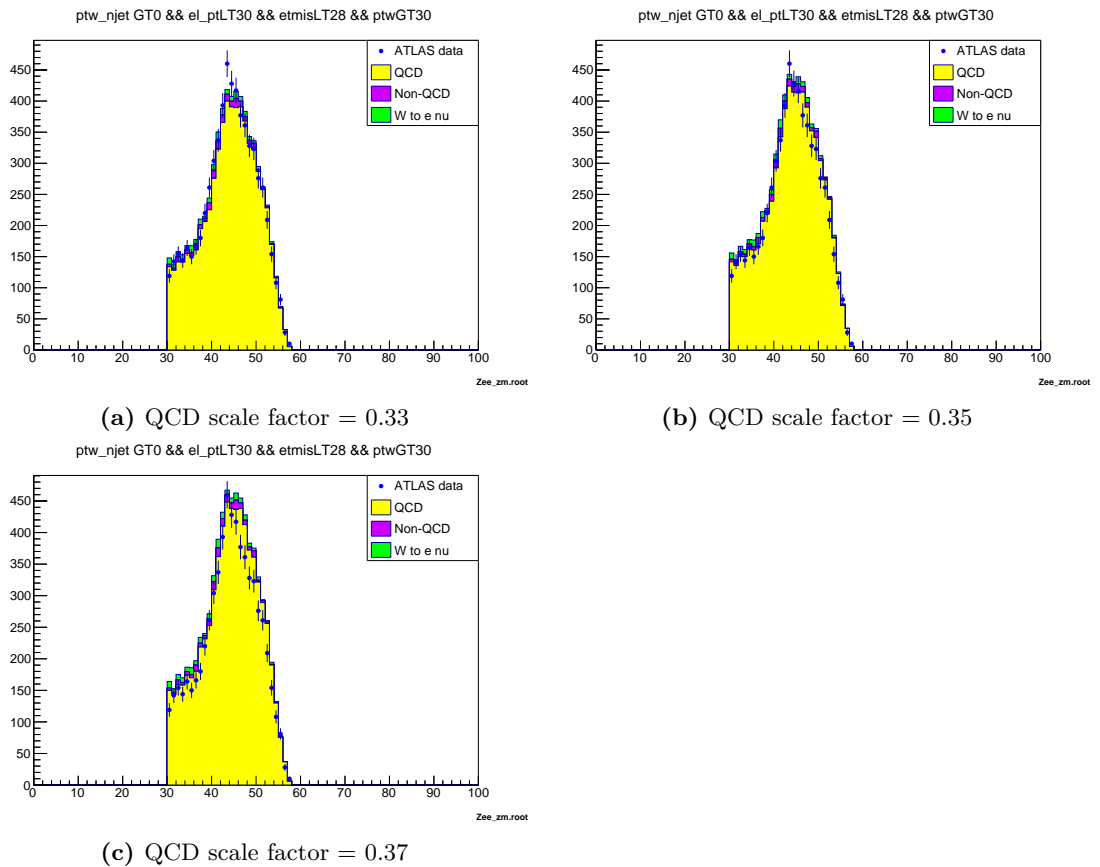


Figure 21: ptw distributions with the cuts $ptw > 30$ GeV, $n_{jet} > 0$, $el_pt < 30$ GeV and $etmis < 30$ GeV for different QCD scale factors

kinematic variables in figures 19 and 20 are examined again. The following cuts were chosen:

Since there are no jets expected in $W \rightarrow e\nu$ events, which can be confirmed when looking at figure 20 where the signal to background ratio decreases significantly as the number of jets increases, the cut `njet == 0` is applied.

Since there is a neutrino present in the W decay, missing transverse momentum/energy \cancel{E}_T is expected in the events. When looking at the `etmis` distribution in figure 24, the background is largest for small \cancel{E}_T . After some trial and error, the cut `etmis > 33 GeV` is chosen.

It is expected, that the W boson itself does not have a large transverse momentum, which can be confirmed when looking at the `ptw` distribution in figure 24. Therefore events with large `ptw` are cut off. The final cut was chosen as `ptw < 35 GeV`.

So the final cut

```
njet == 0 && etmis > 33 && ptw < 35
```

is applied to the `e1_pt` distribution. The distribution of `e1_pt` with the cuts applied can be seen in figure 22. When comparing the `e1_pt` distribution with the cuts and the final QCD scale factor applied, to the `e1_pt` distribution in figure 24, the agreement between simulated and real data is increased whilst the background is decreased significantly. Therefore the applied cuts as well as the QCD scale factor seem to be a decent choice.

el_pt_njet 0 && ptwLT35 && etmisGT33

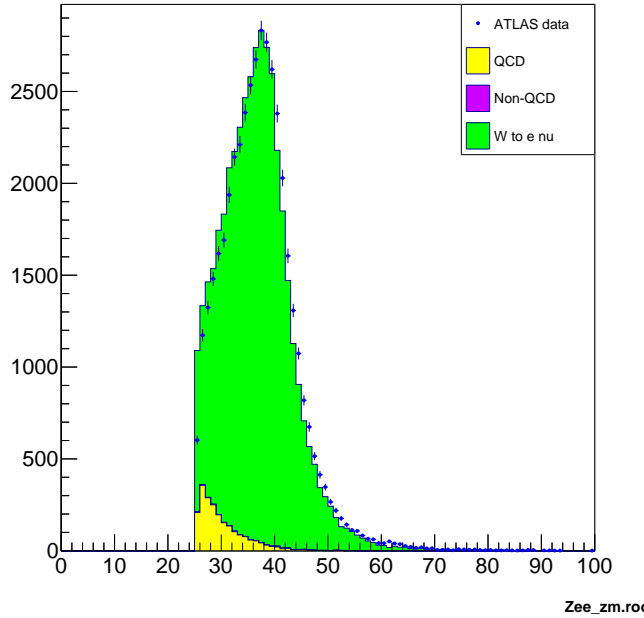


Figure 22: Electron transverse momentum el_pt with the cuts $\text{njet} == 0 \ \&\& \text{etmis} > 33 \ \&\& \text{ptw} < 35$ applied.

11. W boson mass

With the QCD scale factor set, and the cuts to the different kinematic regions applied, the mass of the W boson can now be calculated. This is done with the Jacobi-Peak in the electron transverse momentum distribution el_pt . However, the peak is not very clear, as can be seen in figure 22. This is amongst other things mostly due to decay width of the W boson and the limited resolution of the detector. Therefore a different approach, making use of the half maximum point of the distribution is chosen. The effects of the detector resolution and the decay width of the W boson on the electron transverse momentum distribution are assumed to be symmetric [7]. Therefore even though the peak is not clear in the distribution, the half maximum point should be not change. This assumption is used to extract the W boson mass using the gauge curves.

11.1. Gauge curves

In order to extract the mass of the W boson from the electron transverse momentum distribution, using the half maximum point, the cuts and the QCD scale factor discussed in section 10.2 are applied to the real ATLAS data and simulated $W \rightarrow e\nu$ data sets for different m_W . This is also done for one set of $Z^0 \rightarrow e^+e^-$ data to use as a check whether the fits work in general or just for the W by coincidence. For each of these distributions, the half maximum point is determined using a fit. [7] The distributions with applied

cuts and fits, can be seen in figure 25. Then the W masses of the simulated data sets are plotted against the extracted half maximum of the electron transverse momentum p_T^h in a so called gauge curve. This can be seen in figure 23. The fit used for the gauge curves

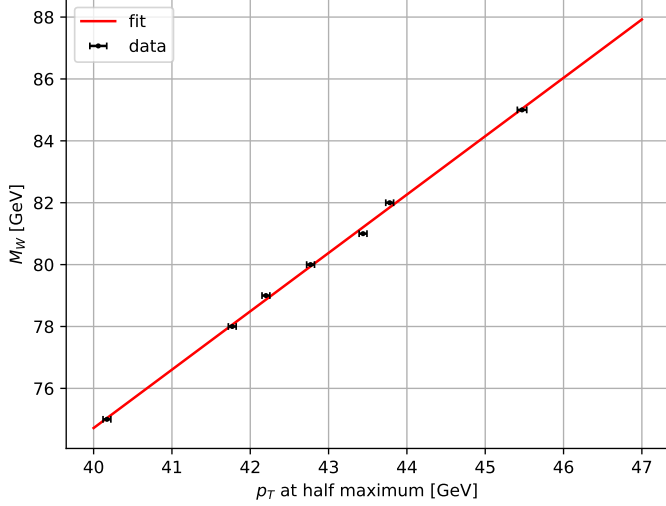


Figure 23: W boson masses from the different data sets plotted against the half maximum points of the Jacobi peak in the electron transverse momentum distribution.

was done with the function

$$M_w(p_T) = a \cdot p_T^h + b \quad (18)$$

In order to obtain the mass of the W boson, the electron transverse momentum at half maximum of the actual ATLAS data has to be inserted into equation 18. For the first set of fits in figure 25 and the resulting gauge curve in figure 23. The fit parameters were determined to

$$a = 1.886 \pm 0.033 \text{ and } b = (-0.732 \pm 1.420) \text{ GeV}$$

The error of parameter b is large compared to the value of b . Since in theory b is expected to be zero, and the fit is done in a range, that is not near zero, the fact that b has such a large error is of course unwanted, but not unexpected. The value of parameter a is somewhat expected as well. Due to the Jacobi peak being located at half the W boson mass, a slope of 2 is expected in theory. Therefore a value of $a = 1.886$ is not far away from that. In order to determine the error of the real W boson mass, the errors of p_T^h , the errors fit parameters as well as their covariance have to be taken into consideration. Using gaussian error propagation, the error of the final W boson mass can be calculated

using

$$\sigma_{M_W}^2 = \left(\frac{\partial M_W}{\partial a} \cdot \sigma_a \right)^2 + \left(\frac{\partial M_W}{\partial b} \cdot \sigma_b \right)^2 + 2 \cdot \frac{\partial M_W}{\partial a} \cdot \frac{\partial M_W}{\partial b} \cdot \sigma_{ab} + \left(\frac{\partial M_W}{\partial p_T^\mu} \cdot \sigma_{p_T^\mu} \right)^2. \quad (19)$$

Here σ_{ab} is the covariance between the fit parameters. It is assumed that p_T^h is not correlated with the errors of a and b . Using the fit which can be seen in figure 23 and equations 18 and 19, the mass of the W boson is calculated to $m_W = (81.037 \pm 0.431) \text{ GeV}$. The same thing can be done for the Z^0 mass, which is calculated to $m_{Z^0} = (91.638 \pm 0.316) \text{ GeV}$.

11.2. Adjusting cuts and fit range

Since the W boson mass calculated in section deviates significantly from the literature value $m_W^{lit} = (80.3692 \pm 0.0133) \text{ GeV}$ [4] the fits to the Jacobi-peaks still needs to be improved. The possible parameters which can be adjusted is the fit range of the fit applied to the Jacobi-peak as well as the readjusting the cuts on the `e1_pt` distributions. Starting with the fit range, the procedure of fitting the Jacobi-peak, creating the gauge curve and extracting the mass of the W and the Z^0 boson, is done for a set off different ranges. A list of the ranges and the corresponding W and Z^0 masses can be seen in table 6

fit range / GeV	m_W / GeV	m_{Z^0} / GeV
30 to 55	81.037 ± 0.431	91.638 ± 0.316
27 to 55	81.068 ± 0.428	91.816 ± 0.321
32 to 55	80.931 ± 0.372	91.782 ± 0.374
32 to 53	80.914 ± 0.451	91.689 ± 0.412
32 to 50	80.884 ± 0.503	91.507 ± 0.377
32 to 60	80.952 ± 0.327	91.958 ± 0.428

Table 6: w and Z^0 boson masses for different fit ranges to to Jacobi-peak fit

Since the calculated value of m_W was closest to the literature value for the range 32 to 55 GeV, this range is chosen for all future fits.

Another way to further increase the quality of the fit is to readjust the cuts applied to the transverse electron momentum distribution. After some initial tries, adjusting the `ptw` did not seem to have any effect on the fit, and cutting on `e1_pt` has the same effect as the the fit range, since the fit range already regulates which values of `e1_pt` are taken into the fit. Therefore the remaining cut is the one on \not{E}_T , meaning that the cut `etmis > 33` which we chose in section 10.3 is adjusted to achieve the best result for the W boson mass. Again the same procedure which was done for the different fit ranges is repeated for different cuts in `etmis`. The cuts, and the corresponding W and Z^0 masses can be seen in table 7

cut selection / GeV	m_W / GeV	m_{Z^0} / GeV
<code>etmis > 35</code>	80.899 ± 0.346	91.339 ± 0.378
<code>etmis > 20</code>	80.252 ± 0.256	91.502 ± 0.314
<code>etmis > 25</code>	80.431 ± 0.278	91.457 ± 0.345
<code>etmis > 24</code>	80.391 ± 0.215	91.441 ± 0.281

Table 7: w and Z^0 boson masses for different cuts on the `etmis`.

The final entry in table 7 is the cut which gave the best result, meaning that m_W is closest to the literature value. To summarize, the final chosen parameters for the calculation of the W boson mass, are the QCD scale factor $c_{QCD} = 0.35^{+0.04}_{-0.05}$ (where $c = 0.35$ was used) and the cuts `njet == 0 && ptw < 35 && etmis > 24` were used to obtain a W and Z^0 boson mass of

$$m_W = (80.391 \pm 0.215) \text{ GeV}$$

$$m_{Z^0} = (91.441 \pm 0.281) \text{ GeV}$$

The fits to the Jacobi-peaks for the final cut selection can be seen in figure 26, and the gauge curve can be seen in figure 27. The fit parameters from the gauge curve fit are $a = 1.876 \pm 0.034$ and $b = (-0.241 \pm 1.453)$ GeV.

12. Systematic uncertainties

The uncertainty given for the mass of the W boson in section 11.2 are entirely statistical. However, systematic uncertainties have to be taken into account as well. There are many sources of systematic uncertainties in the entire process to get the mass of the W boson. The ones which can be evaluated within our means are the calibration of the electron energy, the QCD scale factor, the fit range as well as the cut selection.

12.1. Calibration uncertainty

The systematic uncertainty due to the electron calibration can not be calculated. In order to do so, the entire process of finding the mass of the W boson would need to be repeated for different calibrations, to get an understanding for the impact the calibration has on the final result. This would be beyond the scope of this experiment. Therefore the uncertainty from the calibration of the electron energy can only be estimated. In order to do this, the largest uncertainty of the calculated Z^0 masses is used as uncertainty for the W boson as well. This is not a very accurate way to determine this of uncertainty, it is however not likely, that the W boson uncertainty due to the calibration has a much larger value. Therefore the systematic uncertainty due to the calibration is chosen as ± 0.05 GeV.

12.2. QCD scale factor uncertainty

The QCD scale factor has an impact on the W boson mass, since the background is not fully excluded in the Jacobi-peaks which are used to get p_T^h . This can be seen in figure 22. The background is small compared to the data, but not negligible. Therefore in order to estimate the systematic uncertainty from the QCD scale factor, the analysis would again have to be repeated for different QCD scale factors. Since we were short on time, we were unable to repeat the analysis for different QCD scale factors. So the systematic uncertainty has to be estimated. When looking at figure 22, as mentioned before the QCD background is not negligible. It is however not very large. And the agreement between simulated and real ATLAS data is already quite good. Therefore the effect of the QCD scale factor on the analysis is most likely small even compared to the uncertainty from the calibration. But since this cannot be confirmed, the systematic uncertainty from the QCD scale factor is estimated to ± 0.025 GeV. It is most likely smaller than that, however since it cannot be confirmed a larger value is chosen to not underestimate the uncertainty.

12.3. Fit range uncertainty

Another parameter which was used to optimize the fit was the range. The fit range was adjusted in section 11.2 until the range which resulted in the best W boson mass was found. However when the range was increased or decreased around the half maximum points, the extracted W boson mass got worse. This was explained in section 11.2 with the different W boson masses for different ranges listed in table 6. Therefore the systematic uncertainties due to the fit range is chosen as the difference between the value of m_W for the fit range determined as the best, and the value of the fit range where m_W has the largest difference to that value. The systematic uncertainty from the fit range is therefore ± 0.123 GeV.

12.4. Cut Selection

The systematic uncertainty from the cut selection is estimated similar to the uncertainty of the fit range. The W boson masses for different cut selections are listed in table 7. To estimate the uncertainty, again the difference between the value of m_W for the cut selection which gives the best m_W value, and the m_W value from the cut selection which produces the worst m_W value is chosen as the uncertainty. Therefore the systematic uncertainty due to the cut selection is ± 0.508 GeV.

12.5. Total systematic uncertainty

Although there are more systematic uncertainties, the ones which can be calculated or estimated reasonably well, are listed in table 8. The uncertainty due to the cut selection dominates the other uncertainties. In order to obtain the total systematic uncertainty, that the errors are distributed symmetrically around, and that they are not correlated. In reality this is obviously not true, however this assumption is used, since otherwise the

Systematic uncertainty	Value / GeV
Calibration	± 0.05
QCD scale factor	± 0.025
Fit range	± 0.123
Cut Selection	± 0.508

Table 8: List of systematic uncertainties and their values for the W boson mass.

calculation of the systematic uncertainty would be very difficult and much beyond the scope and available time in this experiment. Therefore this assumption is used, and the systematic uncertainties are added up in quadrature. This leads to the a final result for the measured mass of the W boson of

$$m_W = (80.391 \pm 0.215(\text{stat}) \pm 0.526(\text{sys})) \text{ GeV}.$$

13. Discussion

13.1. Part 1

In this experiment, there are two main part to be studied. First, basics of standard model processes and for this purpose mystery dataset events were investigated. As a result, \cancel{E}_T and neutrino relations, pair production of leptons indicated by the Drell-Yan process, hard scattering processes, hadronization and jets were analyzed. How different elementary particles in standard model reacts with ATLAS detector is also investigated and searched for distinctions. These distinctions were made based on the particle tracks on the detector and kinematic parameters. As a result of the analysis for events in the mystery dataset, some processes were excluded and the remaining were physically justified. Second part based on the measuring the W boson mass and for this energy measurements on ECAL must be calibrated. It was observed that raw energy measurements did not give reliable results and detector calibration was a necessity. The different response of the ECAL modules used in electron energy measurement and the systematic low measurements caused by some energy losses confirmed the need for calibration. $Z \rightarrow e^+e^-$ decays were used for this purpose. The obtained invariant mass distribution was calibrated to be compatible with the Z boson mass in the literature. This accuracy directly contributed to the mass measurement of the W boson.

13.2. Part 2

In the second part of the experiment, the mass of the W boson was determined. In order to do so, different kinematic values were analyzed, to get an understanding of the distributions of data which are actually measured in a detector. From this, the QCD scale and its effect on the distributions of simulated data was analyzed, since the integrated luminosity of the background is unknown. After obtaining the optimal QCD scale factor

to get the best agreement between simulated and real ATLAS data, a cut selection on the kinematic variables was done to reduce the background as much as possible. With the cuts and QCD scale factor applied, the Jacobi-peaks of the transverse electron momentum distributions for different data sets could be extracted using a fit. With these half maximum points and the corresponding W mass, a gauge curve was constructed to obtain the W boson mass of the real ATLAS data set. Different Uncertainties were evaluated and the final result is a W boson mass of

$$m_W = (80.391 \pm 0.215(\text{stat}) \pm 0.526(\text{sys})) \text{ GeV}.$$

This result is very close to the literature value. The uncertainty, especially the systematic uncertainty, is relatively large, due to reasons explained in section 12. Overall the result of the analysis is solid.

A. Appendix

B. A. Muon Energies in the Detectors

Event no.	p_T [Gev/ c]	p [Gev/ c]
1	-38.36 ± 1.016	-85.28
2	33.17 ± 0.797	43.40
4	41.96 ± 0.831	48.89
5	-53.66 ± 2.054	-168.16
6	44.65 ± 1.388	117.32
7	-57.34 ± 1.684	-71.94
8	64.54 ± 2.677	199.91
9	-55.54 ± 1.150	-57.84
11	-37.79 ± 1.185	-100.75
12	37.59 ± 0.653	38.26
13	-59.88 ± 1.766	-105.19
15	-43.88 ± 1.471	-131.69
16	45.66 ± 1.844	152.24
17	-32.65 ± 0.539	-35.23
18	52.80 ± 1.060	54.19
19	-64.49 ± 2.515	-84.75
20	47.56 ± 1.324	104.26
22	52.73 ± 1.304	100.36
23	-44.56 ± 1.470	-117.21

Table 9: Energy Loss measurement data in the Inner Detector

Event no.	p_T [Gev/ c]	p [Gev/ c]
1	-24.06 ± 2.579	-53.92
2	33.35 ± 1.675	43.83
4	38.11 ± 1.333	44.77
5	-61.17 ± 4.417	-177.62
6	36.60 ± 3.150	96.56
7	-51.82 ± 1.070	-64.96
8	64.89 ± 2.846	199.44
9	-48.00 ± 0.948	-50.01
11	-35.03 ± 0.659	-94.11
12	33.85 ± 1.157	34.48
13	-62.15 ± 4.197	-108.68
15	-41.97 ± 2.098	-125.51
16	47.26 ± 2.169	157.69
17	-29.81 ± 0.531	-32.18
18	48.73 ± 2.261	50.00
19	-52.18 ± 1.038	-68.09
20	49.52 ± 3.217	107.98
22	53.09 ± 8.798	101.13
23	-42.55 ± 2.235	-112.26

Table 10: Energy Loss measurement data in the Muon Detector

C. B. Muon Energies in the Detectors

C.0.1. Full η cuts in ElecCalib.c

```
#include "math.h"
#include "TMath.h"

double ElecCalib(double e_raw, double pt, double eta,
                  double phi, double etiso, double eoverp,
                  double mindrjet)
{
    double dummy=pt*eta*phi*etiso*eoverp*mindrjet;
    double energy = e_raw;

    if (0<fabs(eta)<0.2) energy = energy * 91.2/90.14;
    else if (0.2<fabs(eta)<0.4) energy = energy * 91.2/90.1;
    else if (0.4<fabs(eta)<0.6) energy = energy * 91.2/90.07;
    else if (0.6<fabs(eta)<0.8) energy = energy * 91.2/89.79;
    else if (0.8<fabs(eta)<1.0) energy = energy * 91.2/89.47;
    else if (1.0<fabs(eta)<1.2) energy = energy * 91.2/89.50;
    else if (1.2<fabs(eta)<1.4) energy = energy * 91.2/89.48;
    else if (1.4<fabs(eta)<1.6) energy = energy * 91.2/90.10;
    else if (1.6<fabs(eta)<1.8) energy = energy * 91.2/91.25;
    else if (1.8<fabs(eta)<2.0) energy = energy * 91.2/91.27;
    else if (2.0<fabs(eta)<2.2) energy = energy * 91.2/89.03;
    else if (2.2<fabs(eta)<2.4) energy = energy * 91.2/88.11;
    else if (2.4<fabs(eta)<2.5) energy = energy * 91.2/87.77;

    return energy;
}
```

C.0.2. Energy and η cuts in ElecCalib.c

```
#include "math.h"
#include "TMath.h"

double ElecCalib(double e_raw, double pt, double eta,
                  double phi, double etiso, double eoverp,
                  double mindrjet)
{
    double dummy=pt*eta*phi*etiso*eoverp*mindrjet;
    double energy = e_raw;

    if (0.<fabs(eta)<0.5) {
```

```

        if (e_raw<30) energy = energy * 91.2/89.69;
        else if (30<e_raw && e_raw<40) energy = energy * 91.2/89.64;
        else if (40<e_raw && e_raw<50) energy = energy * 91.2/90.53;
        else if (50<e_raw && e_raw<70) energy = energy * 91.2/90.81;
        else if (e_raw > 70) energy = energy * 91.2/90.61;
    }

    else if (0.5<fabs(eta)<1.) {
        if (e_raw<30) energy = energy * 91.2/89.55;
        else if (30<e_raw && e_raw<40) energy = energy * 91.2/89.02;
        else if (40<e_raw && e_raw<50) energy = energy * 91.2/89.77;
        else if (50<e_raw && e_raw<70) energy = energy * 91.2/90.43;
        else if (e_raw > 70) energy = energy * 91.2/90.77;
    }

    else if (1<fabs(eta)<1.5) {
        if (e_raw<30) energy = energy * 91.2/87.49;
        else if (30<e_raw && e_raw<40) energy = energy * 91.2/88.91;
        else if (40<e_raw && e_raw<50) energy = energy * 91.2/87.64;
        else if (50<e_raw && e_raw<70) energy = energy * 91.2/89.37;
        else if (e_raw > 70) energy = energy * 91.2/90.37;
    }

    else if (1.5<fabs(eta)<2.) {
        if (e_raw<80) energy = energy * 91.2/89.81;
        else if (80<e_raw && e_raw<180) energy = energy * 91.2/91.35;
        else if (e_raw > 70) energy = energy * 91.2/91.76;
    }

    else if (2.<fabs(eta)<2.5) {
        if (e_raw<150) energy = energy * 91.2/88.53;
        else if (e_raw > 150) energy = energy * 91.2/88.87;
    }
    return energy;
}

```

C.0.3. Coarse η cuts in ElecCalib.c

```

#include "math.h"
#include "TMath.h"

double ElecCalib(double e_raw, double pt, double eta,

```

```

        double phi, double etiso, double eoverp,
        double mindrjet)
{
    double dummy=pt*eta*phi*etiso*eoverp*mindrjet;
    double energy = e_raw;
    if (0.<fabs(eta)<0.5) energy = energy * 91.2/90.18;
    else if (0.5<fabs(eta)<1.) energy = energy * 91.2/90.12;
    else if (1<fabs(eta)<1.5) energy = energy * 91.2/89.8;
    else if (1.5<fabs(eta)<2.) energy = energy * 91.2/91.22;
    else if (2.<fabs(eta)<2.5) energy = energy * 91.2/88.72;
    return energy;
}

```

D. W-mass

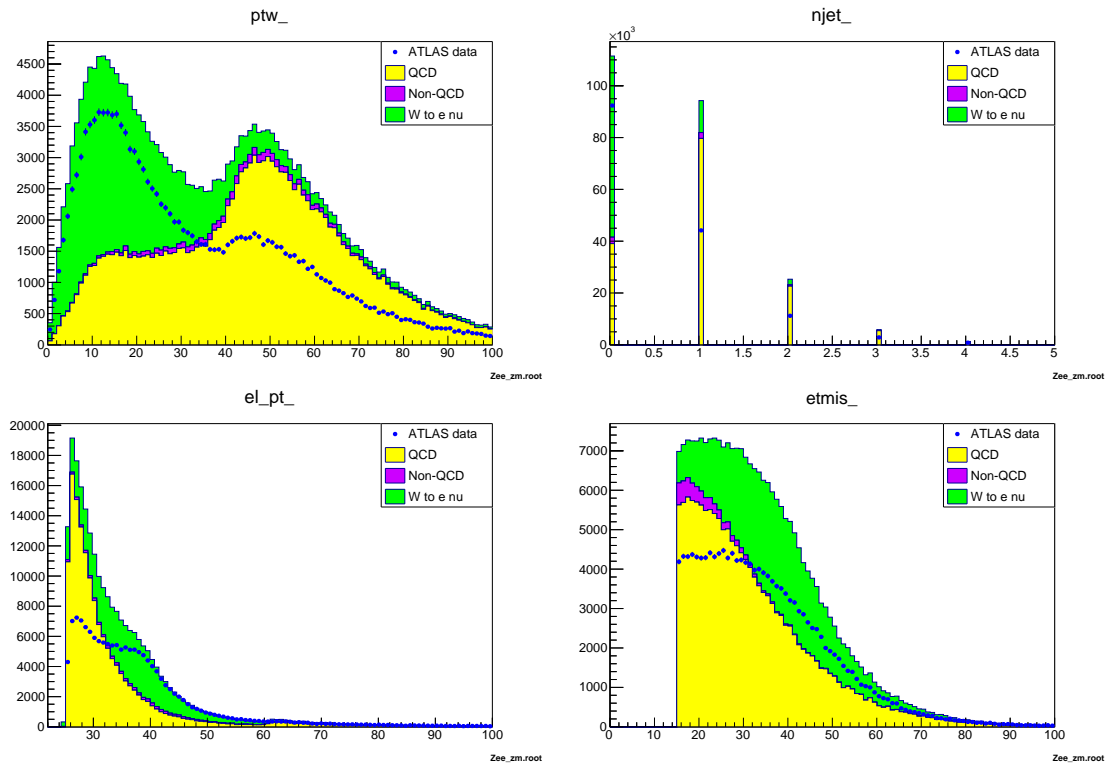


Figure 24: Distributions of the kinematic variables ptw , $njet$, el_pt and $etmis$ for a QCD scale factor of 1

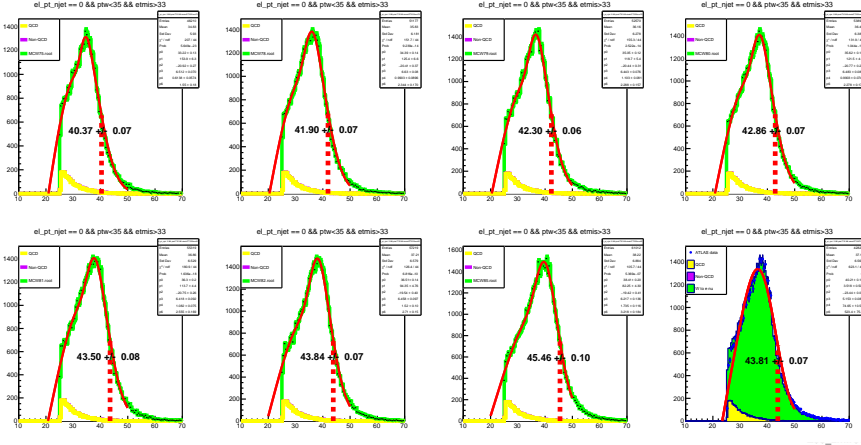


Figure 25: Fits to the Jacobi peak in the electron transverse momentum spectrum for different W masses.

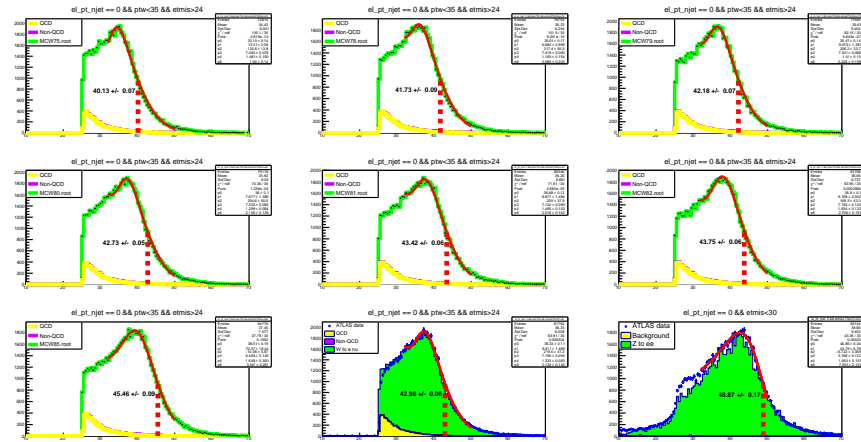


Figure 26: Fits to the Jacobi peak in the electron transverse momentum spectrum for the final set of cuts $n_{\text{jet}} == 0 \&\& ptw < 35 \&\& etmis > 24$.

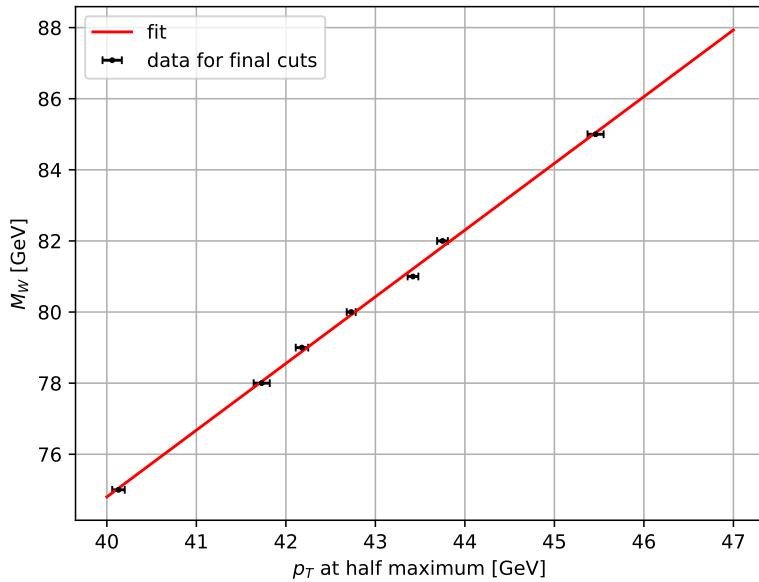


Figure 27: Gauge curve for final set of cuts `njet == 0 && ptw < 35 && etmis > 24.`

References

- [1] I. Adachi, K. Adamczyk, L. Aggarwal, et al. “Measurement of the τ -lepton mass with the Belle II experiment”. In: *Physical Review D* 108.3 (2023), p. 032006. DOI: [10.1103/PhysRevD.108.032006](https://doi.org/10.1103/PhysRevD.108.032006).
- [2] Kazunori Hanagaki et al. “Particle Identification”. In: *Experimental Techniques in Modern High-Energy Physics, A Beginner’s Guide*. Vol. 993. Lecture Notes in Physics. Springer, Jan. 2023, pp. 69–114. DOI: [10.1007/978-4-431-56931-2_6](https://doi.org/10.1007/978-4-431-56931-2_6).
- [3] National Institute of Standards and Technology. CODATA Value: electron mass energy equivalent in MeV. <https://physics.nist.gov/cgi-bin/cuu/Value?mec2mev>. Accessed: 2025-05-24. 2025.
- [4] S. Navas et al. “Review of Particle Physics”. In: *Phys. Rev. D* 110.3 (2024). Particle Data Group, p. 030001. DOI: [10.1103/PhysRevD.110.030001](https://doi.org/10.1103/PhysRevD.110.030001). URL: <https://pdg.lbl.gov>.
- [5] V. V. Shalaev, I. N. Gorbunov, and S. V. Shmatova. “Measurement of Angular Coefficients in the Drell–Yan Process in the CMS Experiment at the LHC”. In: *Physics of Atomic Nuclei* 84.12 (2021), pp. 2037–2040. ISSN: 1063-7788. DOI: [10.1134/S1063778821090313](https://doi.org/10.1134/S1063778821090313).
- [6] M. Tanabashi et al. “Review of Particle Physics”. In: *Physical Review D* 98.3 (2018), p. 030001. DOI: [10.1103/PhysRevD.98.030001](https://doi.org/10.1103/PhysRevD.98.030001).

- [7] University of Bonn, Physics Department. *University of Bonn, Advanced Laboratory Course physics601 E214: The ATLAS Experiment*. Lab Manual. June 2024.